Discover Applied Sciences

Research

Unsymmetricity effects on seismic performance of multi-story buildings

Antony Vimal Paul Pandian[1] · Krishna Prakash Arunachalam[2] · Alireza Bahrami[3] · Lenin Miguel Bendezu Romero[4] · Siva Avudaiappan[2] · Paul O. Awoyera[5]

Received: 22 May 2024 / Accepted: 16 July 2024
Published online: 03 September 2024

Abstract

The unsymmetrical configurations in buildings lead to non-uniform distributions in their strength, mass, and stiffness, and they are consequently prone to damage during seismic hazards. In this study, the seismic performance of multi-story buildings with 5, 8, 10, and 12 stories of square, 'L', 'T', and 'U'-shaped buildings have been investigated. The research deals with the variation of the natural time periods and how it affects the seismic performance of unsymmetrical multi-story buildings. The coupled and uncoupled equations of motion, based on the symmetricity of the buildings about both axes, were solved to obtain natural time periods that influence the spectral acceleration of the ground accelerations. Six important ground accelerations were considered. Nonlinear static analysis, such as pushover analysis, was also carried out on all the buildings. Comparisons were made on the seismic behavior of both the symmetrical and unsymmetrical structures. The results revealed that the spectral acceleration influences dynamic responses, such as base shear, base moment, base torsion, roof displacement, roof rotation, and story drifts of the buildings. Moreover, it was found that even though the 'L'-shaped buildings are unsymmetrical about both axes, they are less vulnerable than the 'T' and 'U'-shaped buildings, which are unsymmetrical about one axis.

Article Highlights

- Due to non-uniform strength, mass, and stiffness distributions, unsymmetrical building configurations amplify seismic vulnerability.
- Study investigates impact of natural time period variations on seismic performance of 5, 8, 10, and 12-story square, 'L', 'T', and 'U'-shaped buildings.
- Findings show that 'L'-shaped buildings, despite being unsymmetrical, have lower seismic vulnerability than 'T' and 'U'-shaped buildings.
- Unequal strength distribution increases roof displacement under seismic loading.
- Varied stiffnesses across structures intensify inter-story drift during earthquakes.

✉ Alireza Bahrami, alireza.bahrami@hig.se; ✉ Paul O. Awoyera, awopaul2002@gmail.com | [1]Department of Civil Engineering, St. Xavier's Catholic College of Engineering, Nagercoil, Tamil Nadu 641062, India. [2]Departamento de Ciencias de La Construcción, Facultad de Ciencias de La Construcción Ordenamiento Territorial, Universidad Tecnológica Metropolitana, Dieciocho 161, Santiago, Chile. [3]Department of Building Engineering, Energy Systems and Sustainability Science, Faculty of Engineering and Sustainable Development, University of Gävle, 801 76 Gävle, Sweden. [4]Department of Civil Engineering, Universidad César Vallejo, Lima, Peru. [5]Department of Civil Engineering, Prince Mohammad Bin Fahd University, Dhahran 34754, Saudi Arabia.

Keywords Response spectrum analysis · Unsymmetrical building · Ground acceleration · Natural time period · Pushover analysis

1 Introduction

An earthquake is the most influencing among the most unpredictable and devastating natural hazards. Multi-story buildings with unsymmetrical configurations are normally constructed nowadays mainly for aesthetic purposes and rapid urbanization growth rate. However, stiffness and mass distribution of such buildings will become non-uniform, and therefore, they will become highly vulnerable during an earthquake. Generally, failures in multi-story buildings made of reinforced concrete are related to structural deficiencies such as quality of materials, detailing, building symmetry, and construction deficiencies. Hence, it is indispensable to evaluate the earthquake behavior of buildings to reduce earthquake-related problems. Over the years, various analytical procedures were developed to ensure the earthquake resistance of the structures whenever they were subjected to significant earthquakes. The earthquake performance of a structure depends on various factors, such as lateral strength, stiffness, and ductility, as well as regular and simple configurations. Out of the above factors, configuration is the important one affecting the performance of a building. Practically, it is rarely possible to have a regular structure, while an irregular structure is very difficult to define. Consequently, a structure's horizontal and vertical building configurations play a very important role in making it seismic resistant during earthquake excitation. The non-uniform distribution of stiffness and mass causes unwanted amplification of maximum displacement and seismic force concentration in a certain region due to unbalanced torsion during earthquake excitation. It may also cause catastrophe for the structure. Therefore, special attention must be paid to designing an irregular building located in a seismic-prone region. Many seismic code books are available that provide the construction aspects and various design requirements for regular buildings to minimize the effects of earthquakes. But such code books are unavailable for elongated and contracted buildings, high-rise structures, structures with irregular configurations, unsymmetrical structures, structures with vertical structural irregularities, etc.

Unsymmetrical buildings have plan irregularity in either x direction or both x and y directions [1]. Unsymmetrical structures suffer from more damage due to earthquakes than their symmetrical buildings. Plan irregularity is one of the most common types of irregularity found nowadays. Horizontal resting elements such as large openings, re-entrant corners, cut-outs, and other abrupt changes or plan irregularities result in torsion, stress concentration, and diaphragm deformations. In the current study, 'L', 'T', 'U', and square-shaped buildings have been taken into account to find their seismic performance during earthquakes. Torsional behavior is one of the main factors that produces damage (reached collapse) on the structures. Torsion is induced in buildings mainly because of the arbitrary stiffness and mass distribution. Generally, torsion is developed in an unsymmetrical building when the distance between the story's center of mass and the story's center of rigidity is larger than 20% of the plan dimension of the structure in either x or y direction. If torsion irregularity occurs, the resistive and inertia forces will act through the center of rigidity and center of mass, respectively [2].

Palagala and Singhal [3] evaluated the earthquake vulnerability of reinforced concrete-framed archetype structures, including vertical irregularity, plan irregularity, short columns, and open-ground stories. HAZUS methodology is used to study the structural score, such as performance point, probability of complete damage, and probability of collapse, of reinforced concrete-framed structure. It was found that the basic score of the reinforced concrete-frame provided with infill made of masonry for the full height was not affected by soil condition.

Khanal and Chaulagain [4] studied the elastic earthquake behavior of 'L'-shaped structural frames through irregular plan dimensions. Buildings of structural irregularities lead to the arbitrary distribution of the story drift, additional torsion, etc., and according to the irregularity type, the structure could fail during an earthquake. The structural responses were measured in terms of story displacement, inter-story drift ratio, torsional irregularity ratio, rotation of torsional diaphragm, normalized base shear, and base moment. This study demonstrated an increase in the irregularity of plan dimensions of the building, which increases the shear force demands, inter-story drifts, and overturning moment at the foundation level.

Kumar and Samanta [5] observed the seismic fragility valuation of existing buildings made of reinforced concrete. The seismic susceptibility is calculated based on the fragility curve obtained. The fragility of 3, 5, and 9-story reinforced concrete structures was studied. The likelihood of damage for structures with a gravity design was indicated to be higher than for buildings with a special moment-resisting frame. Dalal and Dalal [6] studied the reinforced concrete moment-resistant frame's strength, deformation, and fragility. The two seismic analysis techniques employed in this work are the force-based design (FBD) approach and the performance-based plastic design (PBPD) method. Analysis has been done on a 20-story reinforced concrete moment resisting frame. The immediate occupancy (IO), life safety (LS), and collapse prevention (CP) performance standards were all taken into consideration when designing these structural frames. It is understood from the results that the PBPD method performs better than the FBD method in terms of fragility and seismic performance. The LS performance level is suggested for design in the PBPD technique. The inelastic torsional response of unsymmetrical, ductile, reinforced concrete structures with a soft first story was assessed by Hareen and Mohan [7]. The study considers structures of symmetrical rectangular, and unsymmetrical 'L', 'T', and 'U'-plan shapes. More seismic demand is placed on the pliable side corner columns of torsionally irregular, ductile buildings with soft first stories. To prevent premature failure of the column, it was established that the design force should be 1.5 times higher than its design value. Zameeruddin and Sangle [8] discussed the performance-based seismic design. The two main issues are accurate quantification of the unknowns and adequate characterization of the resulting structural destruction for inclusion in the design or performance evaluation technique. Using SAP-2000 software, 15 moment-resisting frames with 4, 6, 8, 10, and 12-story buildings were modeled and investigated with respect to basic periods, roof displacements, inter-story drift ratios, base shears, and modification factors. Eventually, the seismic performance was compared to other limitations.

Sattar [9] evaluated the consistency of the framed structures made of reinforced concrete between prescriptive and performance-based earthquake design methodologies. ASCE 41 was utilized to assess the behavior of reinforced concrete moment resisting frame structures that are 4 and 8 stories in height and were designed in line with ASCE 7–10 norms. The CP and LS performance ratings were used to investigate each component in the archetypal buildings. The archetype structures outperformed at the LS performance level. Cardone and Flora [10] conducted an analysis of multiple inelastic mechanisms. Through the use of various engineering demand parameters like inter-story drift ratios and floor accelerations, a structural investigation was done to assess the seismic demand on the structure. A standard 6-story building that typifies reinforced concrete-frame construction was utilized for the analysis. The plastic mechanism illustrated the structural reactions at various intensity levels and drift profile related to yielding and collapse of the structures. Bhaskar and Menon [11] took various parameters to measure the degree of a building's torsional irregularity. The nonlinear seismic demands on a series of 3D building models were evaluated at various degrees of ground shaking intensity. These models all have similar plan configurations but differ in a variety of ways, including stiffness eccentricity, torsional radius, strength eccentricity, etc. The structures reacted elastically at low intensities. However, it was discovered that strength eccentricity is a superior way to describe torsional irregularity at high-intensity levels in which the building experiences large penetrations into the inelastic behavior.

Dutta et al. [12] examined reinforced concrete buildings that are between low and mid-rise in terms of seismic susceptibility. The damage level was raised by poor design and construction quality and uneven scattering of infill wall. A straightforward nonlinear static analysis-based method was employed to evaluate fragility of low to mid-height reinforced concrete buildings. The pushover analysis was performed by placing a building under a lateral load that increases monotonically. The findings also pointed out a decline in strength and stiffness of the frame without infill wall and reinforced concrete-framed buildings as well as a decline in design and construction quality. Gautam et al. [13] investigated the earthquake fragility properties of reinforced concrete buildings damaged by Nepal's 2015 Gorkha earthquake. The fragility functions depended on in-depth damage inspections of several buildings that were impacted by the earthquake and its aftershocks [14, 15]. Fragility functions are important for estimating overall loss, finding weak points in structures, and mitigating overall risk. They are also valuable at the component level. Infill and parapet walls are two examples of non-structural components that are highly brittle than structural ones and represent a safety danger to building occupants in addition to impairing their ability to use the structure as intended.

Dutta et al. [16] discussed two methods for seismic design of structures. They are the yield point spectra method and the conventional method. The traditional approach maintains stiffness while strength and yield displacement change according to the reduction factor's value. The yield point spectra method is difficult to apply, while the standard method is proven to be safe but unprofitable. The conventional method is suggested, a new iterative strategy that succeeds where the yield spectra-based method fails by producing findings for better ductility. Rahman et al. [17] compared the analysis, design, and earthquake behavior of reinforced concrete buildings under Bangladesh (BNBC-1993), India (IS 1893), and the United States (ASCE 7–10) seismic design regulations. For all codes, a 12-story reinforced concrete special moment-resisting frame was taken into consideration. When ground excitations meant to reflect the Indian design response spectra were applied, the Indian code performed better. Oggu and Gopikrishna [18] examined the susceptibility assessment of 3D-reinforced concrete structural frames under bidirectional single and repeated ground motions. According to the findings of this experiment, the likelihood of the reinforced concrete building collapsing during a series of earthquakes is substantially lower than it would be during a single, extremely powerful earthquake. The building must be constructed to withstand the forces of a series of earthquakes. Bhasker and Menon [19] suggested ground motion intensity measurements (IMs), which exhibit qualities including scaling robustness, effectiveness, sufficiency, and hazard calculability. When compared to those depending on structure-specific measurements, the study's findings expressed that vector IMs, non-structure-specific IMs, are effective insignificantly at estimating the maximum inter-story drift requirement. Hussain and Dutta [20] found that unsymmetrical structures display more sensitive inelastic seismic behavior than symmetrical ones due to the connection of torsional and lateral vibration. The study's general conclusions could be utilized to improve the seismic code's allowance for unsymmetrical construction. Unsymmetrical constructions' torsional and lateral connections make the corner elements more susceptible.

By considering the contributions of higher structural modes, Zain et al. [21] created analytical fragility relationships for reinforced concrete buildings located in highly earthquake-prone regions to minimize computing effort. A comparison of the fragility curves generated by the two techniques was made. The findings demonstrated the efficacy, rigidity, and ease of the established approach for conducting susceptibility calculations without compromising accuracy. For the earthquake design of acceleration-sensitive non-structural components in a building, Surana et al. [22] investigated the floor response spectrum, which was employed to calculate the design floor acceleration. The suggested model to calculate damping modification factors for the elastic floor response spectrum can be used with both the current performance-based earthquake design of non-structural components placed in inelastic building structures and the code-based seismic design. Jalilkhani et al. [23] made a new multi-mode adaptive pushover analysis process to calculate the seismic requirements of reinforced concrete moment-resisting frames. It has been done to analyze four unique reinforced concrete moment resisting building frames with 4, 8, 12, and 20 stories. The findings demonstrated that the multi-mode adaptive pushover analysis process technique can provide an advanced nonlinear static process that is satisfactory for assessing the earthquake behavior of reinforced concrete moment-resisting building frames. In the SPEAR building and the 9-story building, Belejo and Bento [24] looked into the improved modal pushover analysis. A multi-mode method called improved modal pushover analysis offers the benefit of redefining the lateral load imposed. Top displacement ratio, pushover capacity curves, lateral displacement profile, normalized top displacement, inter-story drift, and shear force were employed to assess both structures' seismic vulnerability. Daei and Poursha [25] examined the possibility of applying and soundness of enhanced pushover processes in evaluating the earthquake requirements of mid- and high-rise reinforced concrete structural frames under pulse-like far-fault and near-fault ground excitations. The earthquake demands of reinforced concrete building frames can be reasonably predicted using MPA, EN2, and SMP techniques.

Depending on the 3D performance of a normal three-story reinforced concrete structural frame, Xu and Gardoni [26] provided probabilistic earthquake demand and capacity models. IO, LS, and CP are the three performance levels. This study compared the proposed 3D fragility analysis results to those of the conventional 2D fragility analysis. Cando et al. [27] investigated how stiffness of buildings made of shear walls constructed in accordance with present Chilean rules affected their earthquake performance. Buildings' over-strength and displacement ductility were estimated using pushover analyses, while fragility curves were estimated utilizing incremental dynamic analyses. It was concluded that increasing stiffness enhances the response performance of structures made of reinforced concrete shear wall. Depending on the advocated seismic vulnerability index (SVI) methodology, Kassem et al. [28] suggested a simplified method for assessing the earthquake risk of reinforced concrete buildings. Building frame failure mechanism and the formation of plastic hinges are noted by gradual stress increment. SVI is used to quantify earthquake-related damage to buildings. Zhang and Tian [29] suggested a more straightforward, performance-based, and ideal earthquake design approach for reinforced concrete moment resisting frames that span multiple stories. The design outcomes indicated that compared to the initial design based on strength, 26% of necessary cross-sectional dimensions and 30% of flexural strength can be lowered. The optimized structure was subjected to nonlinear time-history studies utilizing 10 ancient ground accelerations scaled to three levels of earthquake endangerment. The earthquake behavior of four overhead water tanks with several factors, mainly lateral stiffness was evaluated [30], and it was discovered that, compared to filled tanks, empty tanks are far more susceptible to the effects of earthquakes, but this vulnerability might be reduced by providing base isolation. Vimal et al. [31] were involved in finding out the efficacy of base isolation in 5-story buildings of different fundamental natural time periods, and it was resulted that better performance of the building of lower fundamental natural time periods could be obtained if base isolation were provided.

Li et al. [32] evaluated seismic vulnerability of regional group structures using Wenchuan earthquake data from 2008, developing a seismic risk experience database and establishing empirical vulnerability matrices for six types of buildings. A multifactor vulnerability innovation comparison model was made, revealing a decreasing trend in damage with increasing intensity. Si-Qi and Jian [33] reported a quantitative method and innovative model considering composite seismic intensity indicators for estimating regional bridges' seismic risk and vulnerability. The model was updated and validated using 300,000 acceleration records from the Luding earthquake in China, and a vulnerability prediction model was developed using nonlinear regression methods. Si-Qi [34] achieved a novel method for rapidly predicting structural vulnerability utilizing fuzzy decision-making and hierarchical systems. It established rapid fragility prediction models for typical structures, considering multivariate fuzzy membership index. The model considered multiple fuzzy membership parameters and structural earthquake damage database.

Si-Qi et al. [35] proposed a method for assessing seismic risk in urban masonry structures, based on real acceleration records from the Wenchuan earthquake in 2008. The model employed an updated vulnerability level and an innovative seismic risk membership index algorithm, improving the accuracy of seismic risk estimation for masonry structures. Li [36] combined numerical model algorithms with empirical vulnerability methods to develop a prediction model for estimating the fragility of reinforced concrete structures. It used data from the Wenchuan earthquake in China in 2008 and numerical simulation analysis to validate the model's accuracy. The study explored damage modes under different intensities. Li [37] analyzed seismic vulnerability of regional structures during a destructive earthquake in China, analyzing 300,000 acceleration records. It developed an updated structural seismic vulnerability model, a membership index function, and a multidimensional failure prediction model based on an improved mean seismic damage index.

Ruggieri and Vukobratović [38] evaluated acceleration demands in low-rise reinforced concrete buildings with torsion using peak floor accelerations and floor response spectra. The aim was to provide empirical formulas to quantify amplification effects due to torsion in existing and new reinforced concrete buildings. Eight archetype buildings were selected, and numerical models were considered in both linear elastic and nonlinear configurations. The study found that the change of demands depends on the position of the non-structural components and distance between the center of rigidity and center of mass. Ruggieri and Uva [39] examined the extension of linear analysis concepts to nonlinear static analysis procedures in new generation building codes. Nonlinear static analysis is widely employed to assess seismic performance of new and existing buildings but has limitations. Recent upgrades of building codes, like the Italian one, provide different rules for nonlinear static procedures, including the use of a horizontal load profile proportional to story forces. The study investigates the seismic behavior of archetype buildings with increasing height irregularity, using both traditional and new load profiles. The analysis campaign indicates the efficiency of the new load profile and answers the question of whether response spectrum analysis should be extended to nonlinear static analysis.

Based on the past research, it is understood that unsymmetrical plan structures are underperforming than symmetrical structures, and there is hardly any research which concentrates on variation of fundamental natural time period, which is responsible for the dynamic response, and natural time periods of subsequent modes corresponding to various unsymmetrical buildings. Therefore, this research focuses on how natural time period varies based on the type of unsymmetrical buildings.

2 Unsymmetrical buildings

This study examines seismic performance of unsymmetrical shaped buildings such as 'L', 'T', 'U' and symmetrical square-shaped buildings. The plan irregularity is taken as major parameter in the buildings. The plan was drawn in AutoCAD software and is presented in Fig. 1a—d. The bare frame of the square, 'L', 'T', and 'U'-shaped buildings with 5, 8, 10, and 12 stories was developed in the finite element software, ETABS, and the 12-story buildings are depicted in Fig. 2. The

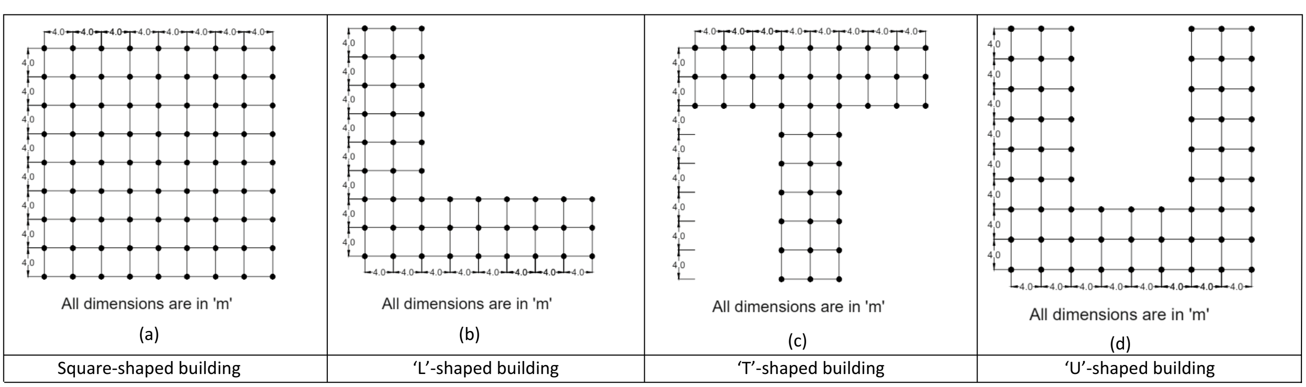

Fig. 1 **a**–**d**. Plans of various unsymmetrical buildings

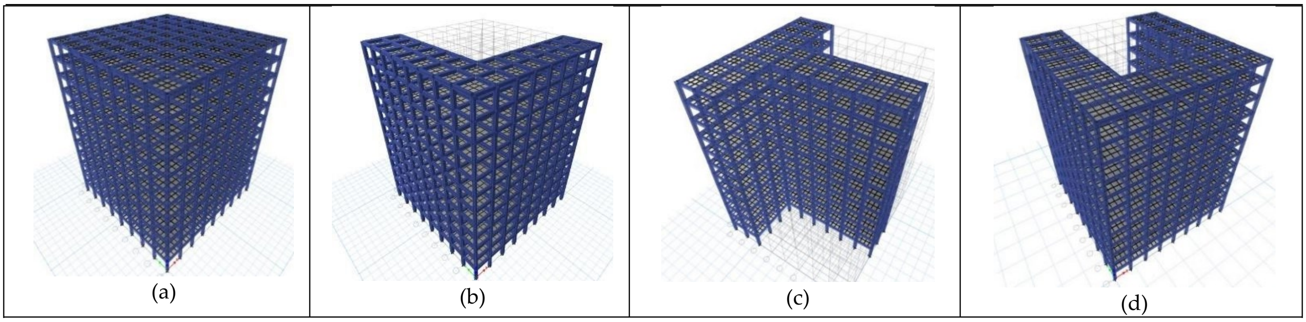

Fig. 2 12-story buildings: **a** square shape, **b** 'L' shape, **c** 'T' shape, and **d** 'U' shape

aforementioned buildings with different 5, 8, 10, and 12 stories are considered for analyzing how other stories of the same building influence seismic performance due to earthquakes. The square-shaped building is treated as reference model as it is regular in mass, stiffness, and strength. The frame selected for the study is special moment-resisting frame. The center of mass and center of rigidity of the irregular buildings do not coincide. On considering 'N' as the number of stories, the square-shaped buildings will have 'N' degrees of freedom (DOF) as they are symmetrical about both axes and the 'T' and 'U'-shaped buildings will have '2N' DOF as they are symmetrical only with respect to x axis. Meanwhile, the 'L'-shaped buildings have '3N' DOF as they are unsymmetrical about both axes. The total seismic weight of structure is taken as 25% of live load and 100% of dead load [41–43]. The concrete mix for all elements is M30 grade and Fe415 rebars were used as longitudinal and confinement reinforcement. The other structural properties, applicable to all the buildings, are listed in Table 1.

Walls are crucial elements in buildings, providing lateral stiffness and contributing significantly to the overall structural behavior. Despite not being prominently presented in figures or diagrams, their presence and influence are typically accounted for in the analytical models and calculations. The exclusion of walls from visual representations or figures does not invalidate the archetype's representation of real-life cases. Instead, it focuses on specific aspects of interest (e.g., plan irregularity and seismic response) while assuming that wall effects are adequately accounted for in the analytical models. Real-life buildings often have complex geometries and structural configurations that may not be fully captured in archetype models. However, archetype buildings are designed to be representative enough to draw meaningful conclusions about structural behavior and performance.

Table 1 Various structural properties of selected multi-story buildings

Sl. No.	Structural properties	Values assigned
1	Story height	3.5 m
2	Length of building	32 m
3	Breadth of building	32 m
4	Bay width	4 m
5	Concrete mix	M30
6	Column size	500 × 500 mm
7	Beam size	300 × 500 mm
8	Slab thickness	120 mm
9	Wall thickness	230 mm
10	Partition wall thickness	100 mm
11	Parapet wall thickness	115 mm
12	Live load on floor	4 kN/m^2
13	Live load on roof	2 kN/m^2
14	Floor finish on floor	1 kN/m^2
15	Floor finish on Roof	0.6 kN/m^2
16	Unit weight of concrete	24 kN/m^3
17	Unit weight of brick	20 kN/m^3

In this research, the archetype reinforced concrete buildings primarily focused on the structural response of reinforced concrete frames under seismic loading conditions. The inclusion of masonry infills was not explicitly modeled in the archetype buildings analyzed. The study aimed to investigate the torsional effects and nonlinear behavior of reinforced concrete structures, focusing on frame elements without incorporating secondary elements like masonry infills. But, the seismic weight of the masonry walls was calculated and considered at each floor level. This approach was chosen to simplify the analysis and isolate the effects of primary structural components. The study focused on capturing ductile behavior in reinforced concrete structures, characterized by significant deformations and energy dissipation capacity beyond yield. This was achieved through the definition of plastic hinges with appropriate yielding force (V_y) and ductility parameters (μ). The modeling approach allowed for the simulation of post-peak behavior, essential for understanding structural response under seismic events. Brittle failure mechanisms, such as shear failures, were not explicitly modeled in this analysis [38].

3 Equation of motion of unsymmetrical building

Table 2 outlines the various parameters used for development of the numerical model.

Building frames in the y axis of an 'L'-shaped unsymmetrical plan are positioned at an eccentric distance ('e') from the diaphragm's center of mass, whereas frames in the x axis are set at an eccentric distance ('d') from the same location. 3DOF, such as roof displacement in *ux* in the x direction, *uy* in the y direction, and torsional rotation in *u*θ in the z direction about the vertical axis, are used to characterize the motion of the roof mass. The x, y, and z axis components of the following equation of motion from Eq. (1.1) are coupled based on the orientation of frames about the center of mass.

$$\begin{bmatrix} m & 0 & 0 \\ 0 & m & 0 \\ 0 & 0 & I_o \end{bmatrix}\begin{bmatrix} \ddot{u}_x \\ \ddot{u}_y \\ \ddot{u}_\theta \end{bmatrix} + \begin{bmatrix} k_{xx} & 0 & k_{x\theta} \\ 0 & k_{yy} & k_{y\theta} \\ k_{\theta x} & k_{\theta y} & k_{\theta\theta} \end{bmatrix}\begin{bmatrix} u_x \\ u_y \\ u_\theta \end{bmatrix} = -\begin{bmatrix} m\ddot{u}_{gx}(t) \\ m\ddot{u}_{gy}(t) \\ I_o\ddot{u}_{g\theta}(t) \end{bmatrix} \tag{1.1}$$

The x axis frames of 'U' and 'T'-shaped unsymmetrical plan buildings are symmetrical about the diaphragm center, while the y axis orientation of the frames is unsymmetrical. This indicates that the structure's response to ground motion in the x direction can be ascertained by solving the single degree of freedom (SDF) system equation. The

Table 2 Various parameters used for development of numerical model

Parameter	Explanation
k_{xx}	X coordinate stiffness
k_{yy}	Y coordinate stiffness
$k_{\theta\theta}$	θ coordinate stiffness
$k_{xaboveN/A}$	Stiffness in x axis above center of gravity
$k_{xbelowN/A}$	Stiffness in x axis below center of gravity
k_{yleft}	Stiffness in y axis for left side frame
k_{yright}	Stiffness in y axis for right side frame
m	Mass matrix
I_o	Moment of inertia of diaphragm mass about vertical axis passing through center of mass
$\ddot{u}_x$, $\ddot{u}_y$, and $\ddot{u}_\theta$	X, y, and θ components of acceleration of center of mass of structure, respectively
$\ddot{u}_{gx}(t)$ and $\ddot{u}_{gy}(t)$	X and y components of ground acceleration, respectively
$\ddot{u}_{g\theta}(t)$	Rotational ground acceleration about vertical axis
ω_n and T_n	Natural frequency and natural time period, respectively
ϕ_{jyn}	Natural mode of vibration in direction y and j^{th} floor level due to n^{th} mode
f_{jyn} and $f_{j\theta n}$	Lateral force and torque at j^{th} floor level, respectively
h_n^*	Effective modal height of n^{th} mode
M_n^*	Effective modal mass of n^{th} mode
V_{bn}, M_{bn} and T_{bn}	Base shear, base moment, and base torsion due to mode n, respectively

equation for the 2DOF system, which is represented in Eq. (1.2), may be solved to find the coupled lateral torsional response of the structure to the ground motion in the y direction.

$$\begin{bmatrix} m & 0 & 0 \\ 0 & m & 0 \\ 0 & 0 & I_o \end{bmatrix}\begin{bmatrix} \ddot{u}_x \\ \ddot{u}_y \\ \ddot{u}_\theta \end{bmatrix}+\begin{bmatrix} k_{xx} & 0 & 0 \\ 0 & k_{yy} & k_{y\theta} \\ 0 & k_{\theta y} & k_{\theta\theta} \end{bmatrix}\begin{bmatrix} u_x \\ u_y \\ u_\theta \end{bmatrix}=-\begin{bmatrix} m\ddot{u}_{gx}(t) \\ m\ddot{u}_{gy}(t) \\ I_o\ddot{u}_{g\theta}(t) \end{bmatrix} \tag{1.2}$$

Symmetrical plan building can be analyzed independently in the two lateral directions of ground motions. The stiffness matrix can be found using a static condensation technique, while the mass matrix is a diagonal matrix containing lumped masses. The equation of motions is uncoupled because the frames are symmetrical about the x and y axes. This means that translation ground motion in either direction would only cause lateral motion of the system in that direction. Equation (1.3) can be employed to solve for the response to each component of ground motion separately. The first line of Eq. (1.3), i.e., $[m][\ddot{u}_x]+[k_{xx}][u_x]=-[m\ddot{u}_{gx}(t)]$ is the traditional basic equation of motion used for obtaining the seismic response and lateral translation u_x of the multistoried building along the x direction. Similarly, the second and third lines of Eq. (1.3) represent the traditional basic equation of motion utilized for obtaining the lateral translation u_y along the y direction and torsional rotation about the vertical axis, respectively.

$$\begin{bmatrix} m & 0 & 0 \\ 0 & m & 0 \\ 0 & 0 & I_o \end{bmatrix}\begin{bmatrix} \ddot{u}_x \\ \ddot{u}_y \\ \ddot{u}_\theta \end{bmatrix}+\begin{bmatrix} k_{xx} & 0 & 0 \\ 0 & k_{yy} & 0 \\ 0 & 0 & k_{\theta\theta} \end{bmatrix}\begin{bmatrix} u_x \\ u_y \\ u_\theta \end{bmatrix}=-\begin{bmatrix} m\ddot{u}_{gx}(t) \\ m\ddot{u}_{gy}(t) \\ I_o\ddot{u}_{g\theta}(t) \end{bmatrix} \tag{1.3}$$

where,

$$k_{xx}=k_{x\,above\,N/A}+k_{x\,below\,N/A}$$

$$k_{yy}=e(k_{y\,right}-k_{y\,left})$$

$$k_{\theta\theta}=\left[e^2\left(k_{y\,right}+k_{y\,left}\right)\right]+\left[\left(\frac{d}{2}\right)^2\times\left(k_{x\,above\,N/A}+k_{x\,below\,N/A}\right)\right]$$

$$k_{\theta x}=\left(\frac{d}{2}\right)\left(k_{x\,below\,N/A}-k_{x\,above\,N/A}\right)$$

$$k_{\theta y}=e(k_{y\,right}-k_{y\,left})$$

The calculated values of the parameters mentioned in Eq. (1) are displayed for the 'L'-shaped building. Its orientation of frames about the center of gravity is delineated in Fig. 3. Translation stiffness of each column is $\frac{12EI}{l^3}$ and is equal to $39.919\times10^3 kN/m$. It consists of 45 columns and hence translation stiffness of each story is equal to $1.796\times10^6 kN/m$. $k_{xx}=k_{yy}$ and is equal to $1.8\times10^6 kN/m$. k_{yx}=k_{xy} and is equal to 0. $k_{\theta x}$ equals to $-0.62\times10^6 kN/m$ and $k_{\theta y}$ equals to $0.62\times10^6 kN/m$. $k_{\theta\theta}$ equals to $369.86\times10^6 kN/m$. The masses of floors and roof are 686 t and 366 t, respectively. The value of $\underline{y}=\underline{x}$ and is equal to $0.3392b$.

4 Response spectrum analysis

Seismic response quantities like base shear, base moment, torsion, roof displacement, and rotation of the unsymmetrical buildings along with the square-shaped buildings of varying heights subjected to six main Indian ground accelerations have been calculated using response spectrum analysis [1]. The selected ground accelerations from Center for Engineering Strong Motion Data (CESMD) along the x as well as y directions are shown in Figs. 4 and 5. The results were compared to that due to design response spectra given in IS 1893 (part 1):2016 [41]. First of all, structural properties of the building, mass as well as stiffness matrices, were defined. Eqs. (2) and (3) have respectively provided

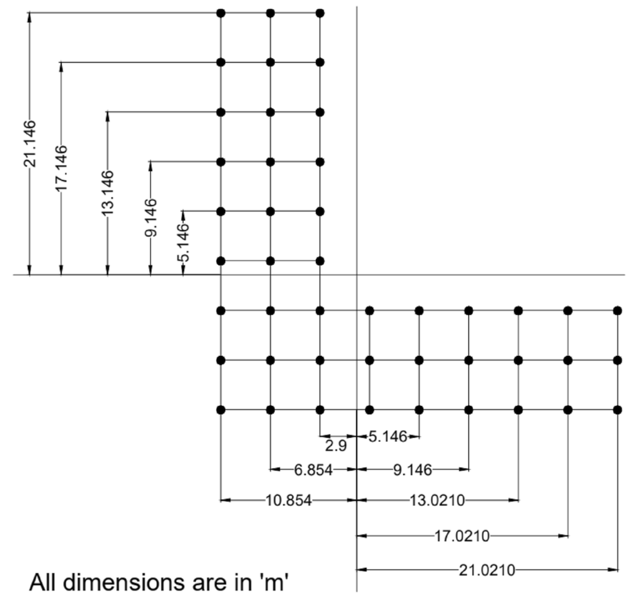

Fig. 3 Orientation of frames about center of gravity

the mass and stiffness matrices of the 'U'-shaped 5-story building, unsymmetrical about the y axis, subjected to ground motion along the y direction. Since the buildings considered are reinforced concrete structures, the damping ratio (ζ_n) of all the modes are taken as 5%. The selected earthquakes are Bhuj earthquake, Uttarkashi earthquake, Chamba earthquake, Chamoli earthquake, NE-INDIA earthquake (India Burma), and NE-INDIA earthquake, along with the IS 1893:2016 (rocky soil). For these earthquake ground motions, Prism software forms the elastic response spectrum. Table 3 presents the peak ground motions in the y direction.

$$[m] = \begin{bmatrix} m_1 & 0 & 0 & 0 & 0 & 0 & 0 & 0 & 0 & 0 \\ 0 & m_2 & 0 & 0 & 0 & 0 & 0 & 0 & 0 & 0 \\ 0 & 0 & m_3 & 0 & 0 & 0 & 0 & 0 & 0 & 0 \\ 0 & 0 & 0 & m_4 & 0 & 0 & 0 & 0 & 0 & 0 \\ 0 & 0 & 0 & 0 & m_5 & 0 & 0 & 0 & 0 & 0 \\ 0 & 0 & 0 & 0 & 0 & I_{O1} & 0 & 0 & 0 & 0 \\ 0 & 0 & 0 & 0 & 0 & 0 & I_{O2} & 0 & 0 & 0 \\ 0 & 0 & 0 & 0 & 0 & 0 & 0 & I_{O3} & 0 & 0 \\ 0 & 0 & 0 & 0 & 0 & 0 & 0 & 0 & I_{O4} & 0 \\ 0 & 0 & 0 & 0 & 0 & 0 & 0 & 0 & 0 & I_{O5} \end{bmatrix} \tag{2}$$

$$[k] = \begin{bmatrix} k_{yy1} & -k_{y2} & 0 & 0 & 0 & k_{y\theta11} & -k_{y\theta2} & 0 & 0 & 0 \\ -k_{y2} & k_{yy2} & -k_{y3} & 0 & 0 & -k_{y\theta2} & k_{y\theta22} & -k_{y\theta3} & 0 & 0 \\ 0 & -k_{y3} & k_{yy3} & -k_{y4} & 0 & 0 & -k_{y\theta3} & k_{y\theta33} & -k_{y\theta4} & 0 \\ 0 & 0 & -k_{y4} & k_{yy4} & -k_{y5} & 0 & 0 & -k_{y\theta4} & k_{y\theta44} & -k_{y\theta5} \\ 0 & 0 & 0 & -k_{y5} & k_{yy5} & 0 & 0 & 0 & -k_{y\theta5} & k_{y\theta55} \\ k_{\theta y11} & -k_{\theta y2} & 0 & 0 & 0 & k_{\theta\theta1} & -k_{\theta2} & 0 & 0 & 0 \\ -k_{\theta y2} & k_{\theta y22} & -k_{\theta y3} & 0 & 0 & -k_{\theta2} & k_{\theta\theta2} & -k_{\theta3} & 0 & 0 \\ 0 & -k_{\theta y3} & k_{\theta y33} & -k_{\theta y4} & 0 & 0 & -k_{\theta3} & k_{\theta\theta3} & -k_{\theta4} & 0 \\ 0 & 0 & -k_{\theta y4} & k_{\theta y44} & -k_{\theta y5} & 0 & 0 & -k_{\theta4} & k_{\theta\theta4} & -k_{\theta5} \\ 0 & 0 & 0 & -k_{\theta y5} & k_{\theta y55} & 0 & 0 & 0 & -k_{\theta5} & k_{\theta\theta5} \end{bmatrix} \tag{3}$$

The natural frequencies (ω_n) and mode shapes (ϕ_n) of the Eigen value problem are determined by solving the characteristic equation utilizing MATLAB tool. The corresponding natural time periods are calculated using the relation $T_n = 2\pi/\omega_n$. It is followed by the computation of the peak response in the every n^{th} mode, where n = 1, 2,…, N

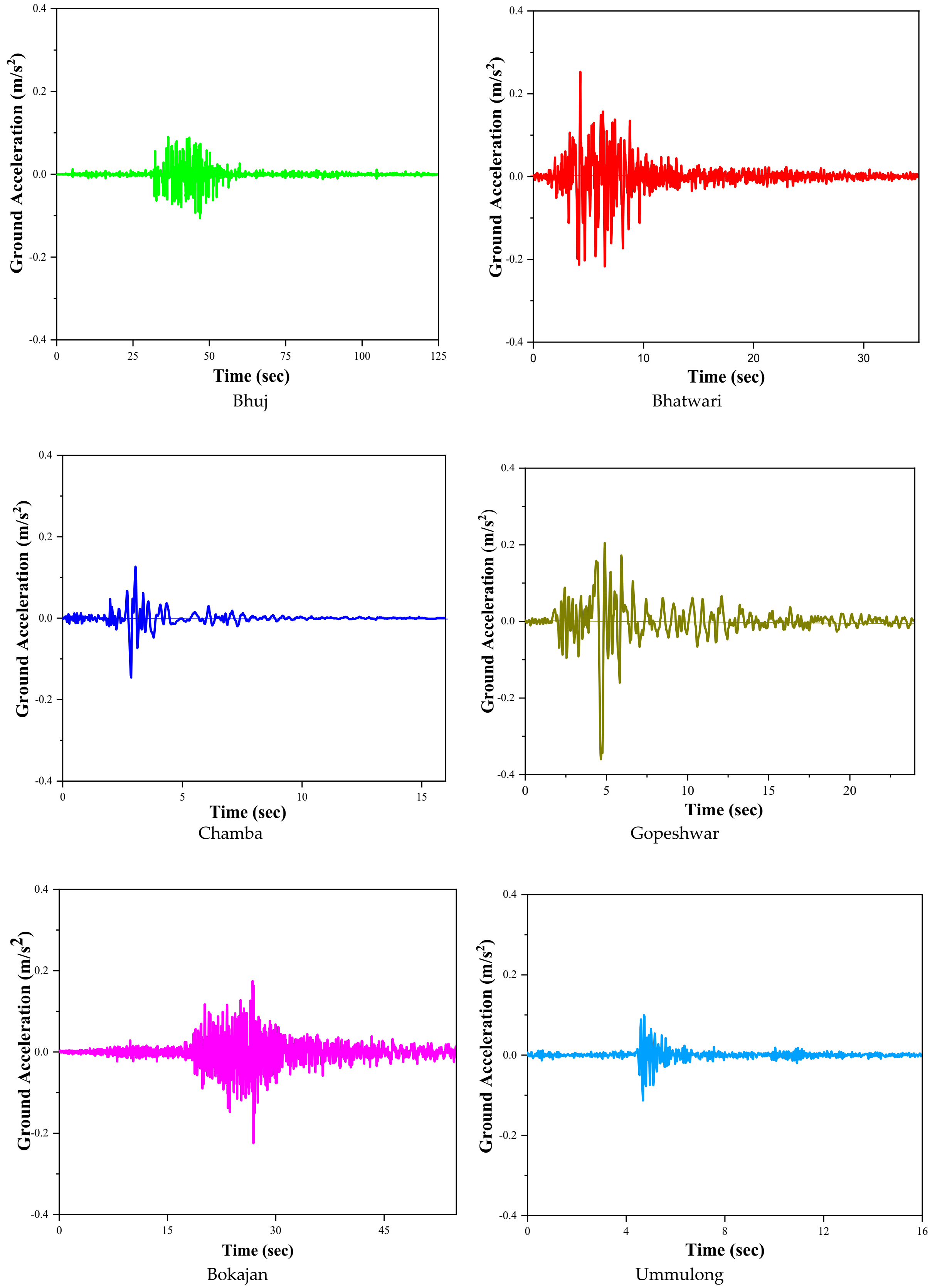

Fig. 4 Various ground accelerations in x direction

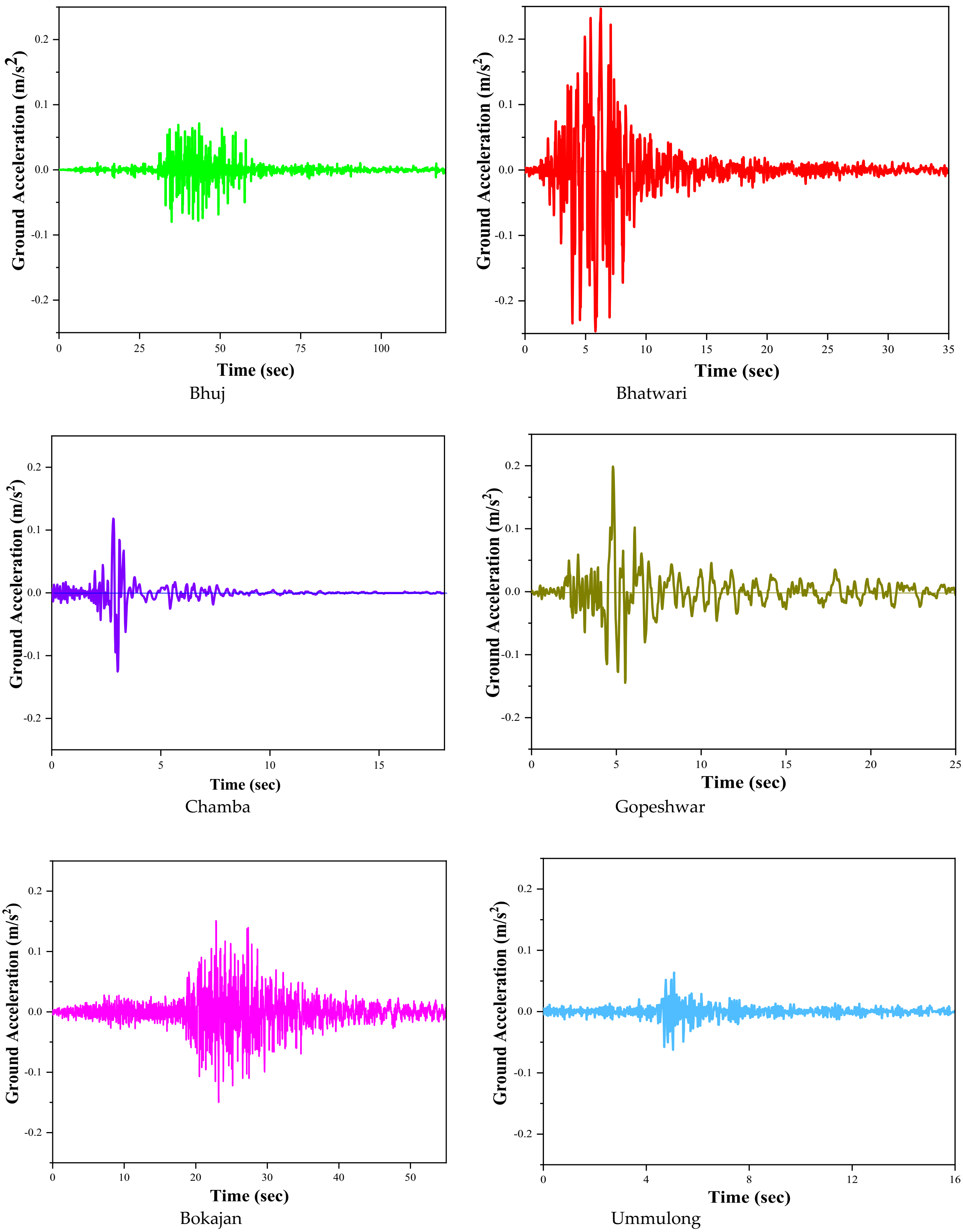

Fig. 5 Various ground accelerations in y direction

Table 3 Peak ground motions in y direction

Earthquake name	Magnitude	Date	Station	Hypocentral distance (km)	Peak ground acceleration (m/s^2)	Peak ground velocity (mm/s)	Peak ground displacement (mm)	Site geology
Bhuj earthquake	7.7	26/01/2001	Ahmedabad	239	1.0382	112.72439	186.39396	Soil
Uttarkashi earthquake	7.0	20/10/1991	Bhatwari	21.7	2.4800	168.88370	603.18375	Rock
Chamba earthquake	4.9	24/03/1995	Chamba	34	1.4284	74.3389	58.55796	Soil
Chamoli earthquake	6.6	29/03/1999	Gopeshwar	17.3	3.5283	456.09240	162.20788	Rock
NE-INDIA earthquake	7.2	06/08/1988	Bokajan	189.9	2.2000	109.12007	1170.06654	Soil
NE-INDIA earthquake	4.5	10/09/1986	Ummulong	44.9	1.1100	33.47926	98.62966	Rock

for the square-shaped building, and n = 1, 2,…, 2N for the 'T' and 'U'-shaped buildings, and n = 1, 2,…, 3N for the 'L'-shaped buildings. Spectral deformation (D_n) and pseudo spectral acceleration (A_n), corresponding to the natural time period T_n and damping ratio ζ_n each mode is read out from each ground acceleration's deformation and acceleration response spectra. The lateral deformations and rotations of the floors due to each mode are computed employing Eqs. (4) and (5).

$$u_{jyn} = \Gamma_n \phi_{jyn} D_n \tag{4}$$

$$u_{j\theta n} = \Gamma_n \phi_{j\theta n} D_n \tag{5}$$

The equivalent static forces, which are lateral forces f_{yn} and $f_{\theta n}$, are calculated by Eqs. (6) and (7), respectively. Subsequently, the base shear (V_{bn}), base moment (M_{bn}), and base torsion (T_{bn}) are calculated by static analysis of the structural frame subjected to external forces f_{yn} and $f_{\theta n}$ utilizing Eqs. (8), (9), and (10), respectively.

$$f_{jyn} = \Gamma_n m_j \phi_{jyn} A_n \tag{6}$$

$$f_{j\theta n} = \Gamma_n r^2 m_j \phi_{j\theta n} A_n \tag{7}$$

$$V_{bn} = M_n^* A_n \tag{8}$$

where, $A_h = \frac{S_a}{g} \frac{I}{R} \frac{Z}{2}$

$$M_{bn} = h_n^* M_n^* A_n \tag{9}$$

$$T_{bn} = I_{on}^* A_n \tag{10}$$

where, M_n^* is the effective modal mass of mode 'n' and h_n^* is the effective modal height mode 'n'. The complete quadratic combination (CQC) model combination rule was adopted, since the natural time periods of the modes are closely spaced. The total seismic response due to all the significant modes are calculated employing Eq. (11). Even though all the modes' contributions were considered in calculating the seismic responses, only the first few modes noticeably contributed.

$$r_0 = \sqrt{\left(\sum_{i=1}^{N} \cdot \sum_{n=1}^{N} \rho_{in} r_{io} r_{no} \right)} \tag{11}$$

where, $\rho_{in} = \frac{\zeta^2 (1+\beta_{in})^2}{(1-\beta_{in})^2 + 4\zeta^2 \beta_{in}}$

5 Pushover analysis

With pushover analysis, a type of nonlinear static analysis, a building's seismic performance may be essentially determined by simply applying incremental lateral force until the structure collapses. The pushover curve is a crucial tool for determining damage limit states and obtaining seismic behavior. A pushover curve is plotting a deflection parameter dependent on strength. Based on the performance of the structure, a plot versus plastic rotation may be created to indicate the strength level attained in specific members to the lateral displacement at the top of the structure or bending moment. Pushover study findings provide the load level, deflection ductile capacity, and structural system mechanism for failure. An element (or group of elements) reaching a lateral deformation level at which significant strength degradation begins then performance level can be measured, as illustrated in Fig. 6.

Fig. 6 Performance level

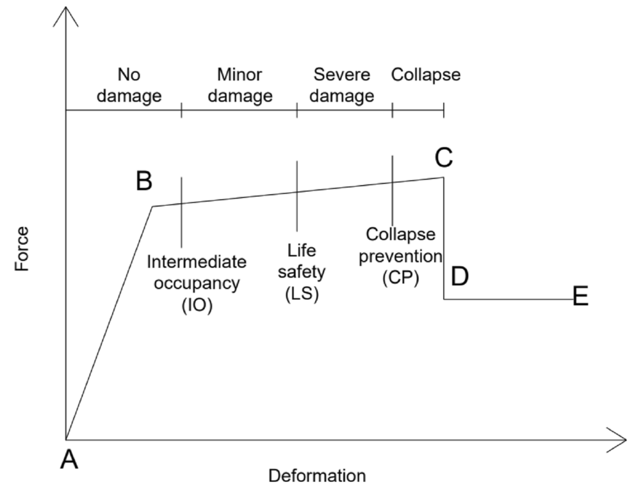

6 Results and discussion

The results based on base shear, base torsion, base moment, story displacement, inter-story drift, roof displacement, and roof rotation of buildings of unsymmetrical plan are discussed along with building of symmetrical plan. The center of the mass and stiffness matrices do not coincide with the center of gravity of buildings due to irregular planning.

6.1 Fundamental natural time period and mode shapes

Regarding the square-shaped building, its plan is symmetrical about both axes, therefore, the equation of motion, i.e., Eq. (1) can be detached in both the x and y axes. Moreover, torsional effects will not be there. These leads an 'N'-story square-shaped building to have 'N' DOF. Meanwhile, the 'T' and 'U'-shaped buildings are symmetrical about the x axis and unsymmetrical about the y axis. While uncoupled equation can be made along the x direction, both lateral translations along the y axis and torsional moment are coupled in the y direction. Therefore, DOF along the y direction will be 2N for an 'N'-story 'T' as well as 'U'-shaped building. Interestingly, the 'L'-shaped building is unsymmetrical about both the x and y directions, consequently, the lateral translation along the x and y directions and torsional moment are coupled along both the x and y directions. Therefore, DOF of an 'N'-story 'L'-shaped building will be 3N in both the x and y directions. For example, DOF of the 5-story 'U' and 'L'-shaped buildings are 10 and 15, respectively. Their characteristic equation is

Table 4 Natural time periods of all buildings

Sl. No.	Natural time period	Type of building															
		Square-shaped building				'L'-shaped building				'T'-shaped building				'U'-shaped building			
		No. of story				No. of story				No. of story				No. of story			
		5	8	10	12	5	8	10	12	5	8	10	12	5	8	10	12
1	T_1	0.416	0.655	0.816	0.976	0.396	0.632	0.786	0.948	0.395	0.629	0.786	0.948	0.531	0.832	1.032	1.233
2	T_2	0.143	0.221	0.274	0.327	0.395	0.629	0.786	0.937	0.355	0.564	0.707	0.848	0.451	0.707	0.878	1.049
3	T_3	0.092	0.136	0.167	0.198	0.362	0.576	0.721	0.863	0.136	0.213	0.264	0.316	0.183	0.281	0.347	0.413
4	T_4	0.073	0.101	0.122	0.144	0.137	0.213	0.265	0.317	0.122	0.191	0.237	0.284	0.155	0.239	0.295	0.351
5	T_5	0.065	0.083	0.098	0.115	0.136	0.212	0.264	0.315	0.088	0.131	0.161	0.192	0.117	0.173	0.212	0.251
6	T_6	–	0.073	0.084	0.097	0.125	0.195	0.242	0.289	0.079	0.118	0.145	0.172	0.099	0.147	0.180	0.213
7	T_7	–	0.067	0.075	0.085	0.088	0.131	0.161	0.192	0.069	0.097	0.118	0.139	0.092	0.128	0.155	0.182
8	T_8	–	0.064	0.069	0.077	0.087	0.131	0.161	0.191	0.063	0.087	0.106	0.125	0.082	0.109	0.132	0.155
9	T_9	–	–	0.065	0.071	0.080	0.120	0.148	0.175	0.062	0.080	0.095	0.111	0.078	0.105	0.125	0.145
10	T_{10}	–	–	0.063	0.067	0.070	0.097	0.118	0.140	0.056	0.072	0.085	0.100	0.070	0.092	0.106	0.123

solved using MATLAB to get the natural frequencies and mode shapes after the formation of corresponding mass and stiffness matrices. Mass and stiffness matrices of the 'U'-shaped building are provided in Eqs. (2) and (3). Table 4 presents natural time periods of all the buildings subjected to ground excitation along the y direction. It shows that when the number of stories of any building increases, natural time period gradually increases. For example, fundamental natural time periods of the 5th, 8th, 10th, and 12th stories of the 'T'-shaped building are 0.395 sec, 0.629 sec, 0.786 sec, and 0.948 sec, respectively. While the 'L'-shaped building demonstrates lowest fundamental natural time periods among all the buildings, it is the 'U'-shaped building exhibiting highest fundamental natural time periods. Except the first few modes, remaining modes of all the buildings mark their corresponding natural time periods are highly closed. As a conclusion, the modal combination rule, CQC, is used instead of square root of summation of squares for calculating the total seismic responses from the individual modal responses.

6.2 Spectral acceleration and spectral displacement

PRISM software constructed the response spectrum for all the above ground accelerations. The spectral acceleration coefficient was obtained from the above response spectrum for a particular value of natural time period and damping ratio, in addition to the elastic response spectrum from IS 1893 (part 1):2016. The acceleration spectrum decreases as natural time period lengthens, and the displacement spectrum increases proportionally to natural time period. For example, natural time periods of the five modes of the 5-story square building are 0.416 sec, 0.143 sec, 0.092 sec, 0.073 sec, and 0.065 sec. The corresponding values of spectral displacement are 7.564 mm, 1.013 mm, 0.370 mm, 0.235 mm, and 0.197 mm, respectively, and spectral accelerations are 0.173 g, 0.208 g, 0.177 g, 0.179 g, and 0.188 g, respectively. This indicates that spectral displacement is varying directly proportional to natural time period and vice versa to spectral acceleration. Acceleration as well as displacement response spectra for the various ground accelerations in the x and y directions are depicted in Fig. 7a and b. Spectral acceleration response spectra for various ground acceleration have been matched with response spectra for rocky soil from IS 1893:2016, as shown in Fig. 7.

6.3 Base shear

Base shear is an estimate of maximum expected lateral force that will occur due to seismic ground motion at the base of the structure. Base shear is affected by the unsymmetrical plan of the building, in addition to weight of the structure and ground acceleration. The total seismic response of base shear is obtained by multiplying both dynamic and static responses. Static response is proportional to seismic weight of the building and dynamic response is nothing but the spectral acceleration (Sa/g) from the response spectrum of each ground acceleration. Seismic weights of the 5, 6, 7, and 8-story buildings are respectively equal to 6042 kN, 9918 kN, 12502 kN, and 15086 kN, irrespective of the shape of the buildings. Static response is linearly increasing from 5 to 12 stories of a particular building. For example, model static responses of the 5-story square building subjected to Bhuj ground acceleration are 5336.726 kN, 520.090 kN, 138.621 kN, 39.506 kN, and 7.125 kN, respectively, and dynamic responses, i.e., design horizontal acceleration seismic coefficients, are 0.091, 0.110, 0.094, 0.095, and 0.100, respectively. Design horizontal acceleration seismic coefficient (A_n) is obtained from spectral acceleration $\left(\frac{S_a}{g}\right)$, in which, the values of the zone factor (Z), importance factor (I), and response reduction factor (R) are taken as 0.36, 1.5, and 5, respectively. After multiplying these two responses, base shears are achieved for the five individual modes as 487.982 kN, 57.298 kN, 12.962 kN, 3.736 kN, and 0.709 kN. Total base shear is calculated using the CQC modal combination rule and is equal to 492.319. Total base shears of other 5-story buildings are delineated in Table 5, and the comparison of base shears of all the buildings having different stories are displayed in Fig. 8. In all different-story buildings, the square-shaped building is giving maximum base shear when compared to other shaped buildings. Base shears of the 5th, 8th, 10th, and 12th stories of the square-shaped buildings subjected to Bhuj ground acceleration are respectively 8.15%, 8.55%, 11.85%, and 9.11% of seismic weight. From the 5th story to 10th story, base shear increases, however, it decreases toward the 12th story. Even though the static response of the 12-story square-shaped building is maximum, its dynamic response, i.e., spectral acceleration, of the first two modes is significantly less than that of a 10-story building. This is the reason behind the reduced base shear of the 12-story building; the same issue is valid for remaining buildings of different shapes. After the square-shaped building, it is the 'U'-shaped building providing maximum base shear almost in all the story levels. Even though the 'L'-shaped building is unsymmetrical about both axes, it demonstrates less value of base shear, and base shears of both the 'L' and 'T'-shaped buildings are tantamount approximately. As far as modal contribution is concerned, the first mode contributes nearly 99% of total response for

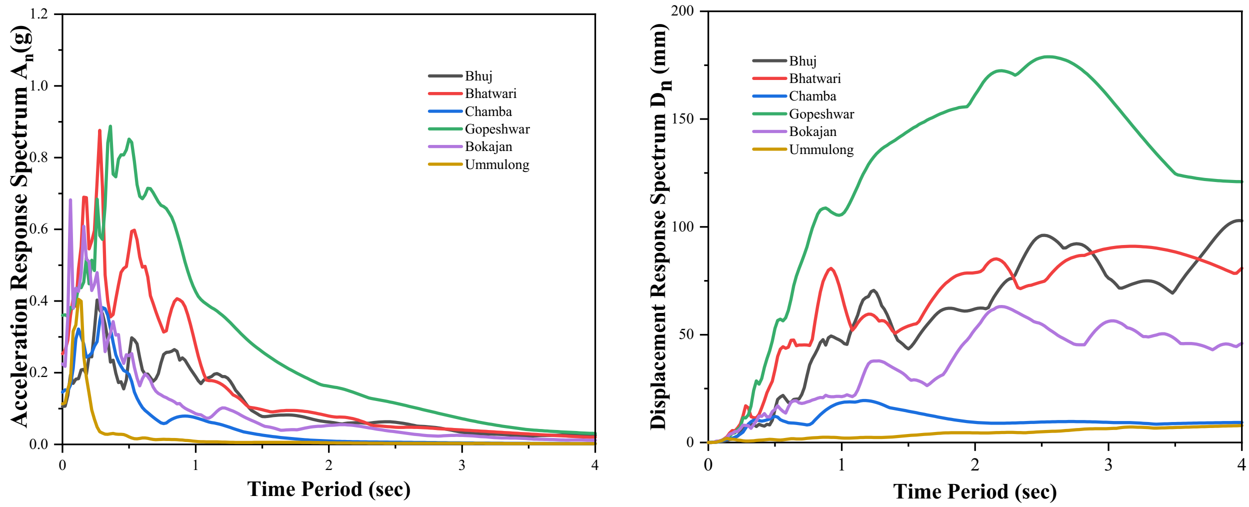

(a) Spectral acceleration and displacement for ground accelerations in y direction

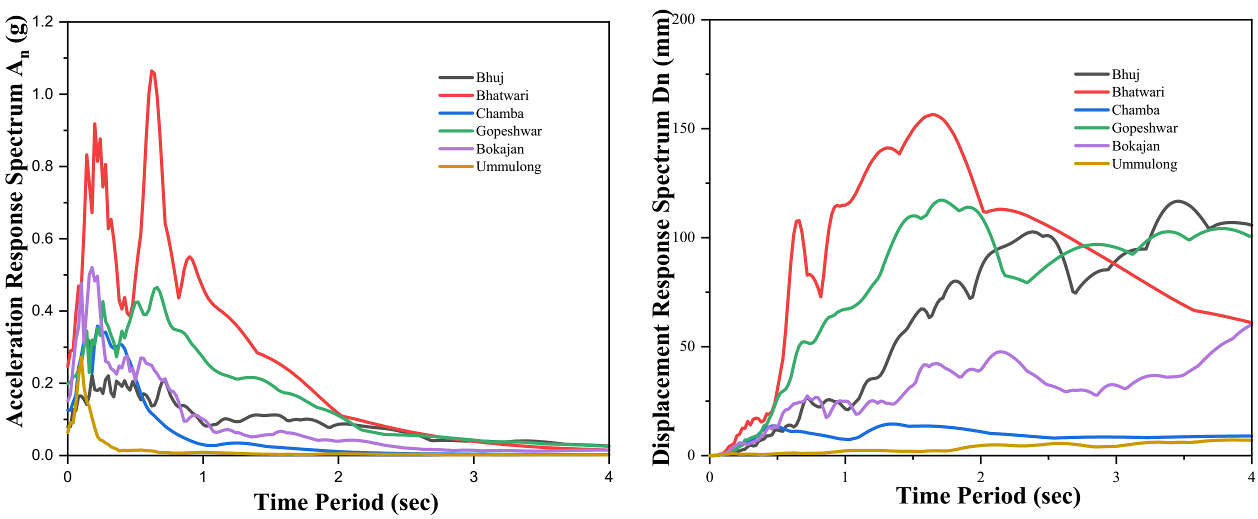

(b) Spectral acceleration and displacement for ground accelerations in x direction

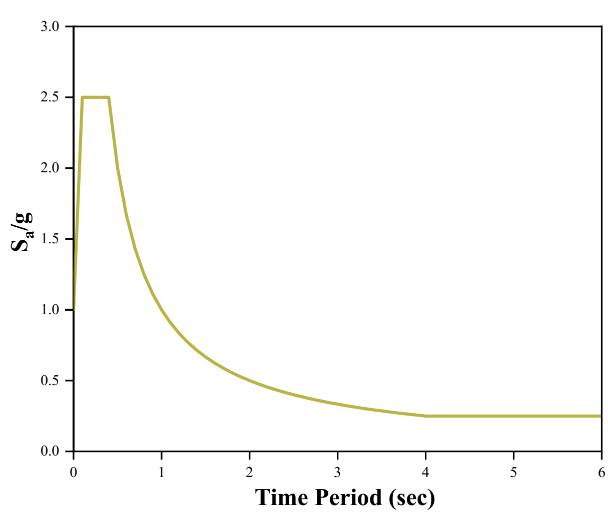

Fig. 7 Response spectra from IS 1893:2016 (rocky soil)

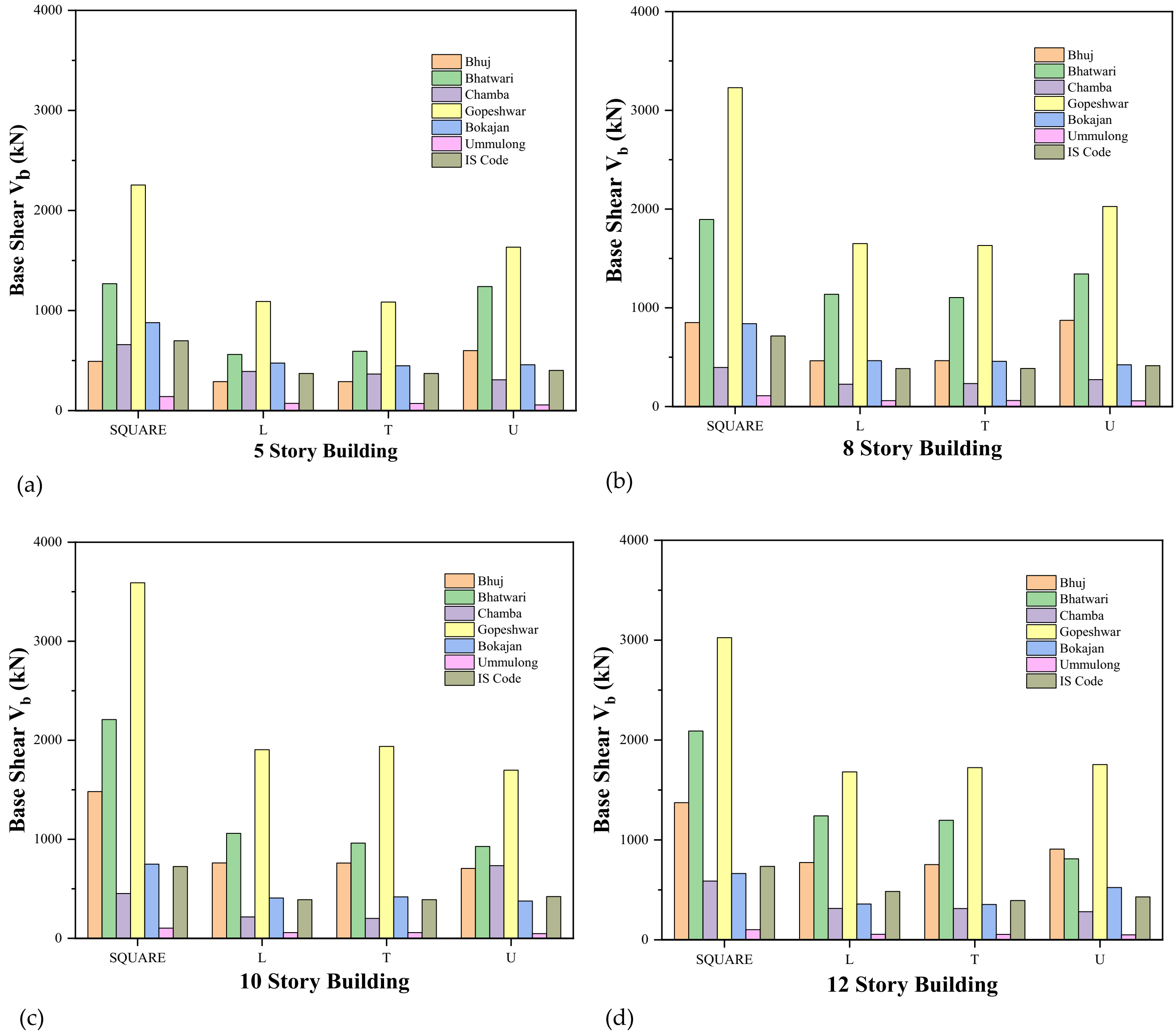

Fig. 8 Base shears for ground accelerations in y direction

the 'U', 'T', and square-shaped buildings, and it is the first two modes giving the same amount for the 'L'-shaped building.

Gopeshwar ground motion provided higher base shear than Bhatwari, Bhuj, and Bokajan ground motions. Fig. 8 illustrates that Chamba and Ummulong ground motions provide less seismic response than the one given as per IS 1893:2016. On comparing the overall performance, it is Gopeshwar's ground motion exhibiting maximum base shear in the 10-story square-shaped building, which is equal to 3590.041 kN. It is 28.716% of seismic weight. Fig. 8 indicates that there is no considerable increment in base shear based on increment in the number of stories due to certain ground motion, such as Bokajan, Ummulong, and IS code. The reason is that the increased static response is balanced by reduced dynamic response, mainly due to highly randomly distributed spectral acceleration, which depends on natural time period for a fixed damping ratio. Therefore, it is determined that square building is highly vulnerable among all the considered and out of the unsymmetrical buildings. It is the 'U'-shaped building highly susceptible to earthquake for the 5th and 8th stories, and almost all the unsymmetrical buildings perform well for the 10th and 12th stories. It is also depicted that the 'L', 'T', and 'U'-shaped buildings are alternatively sensitive for varying earthquakes. Base shear in the 'L', 'T' and 'U'-shaped buildings decreases by 30%, unlike the square-shaped building where base shear decreases by 40%.

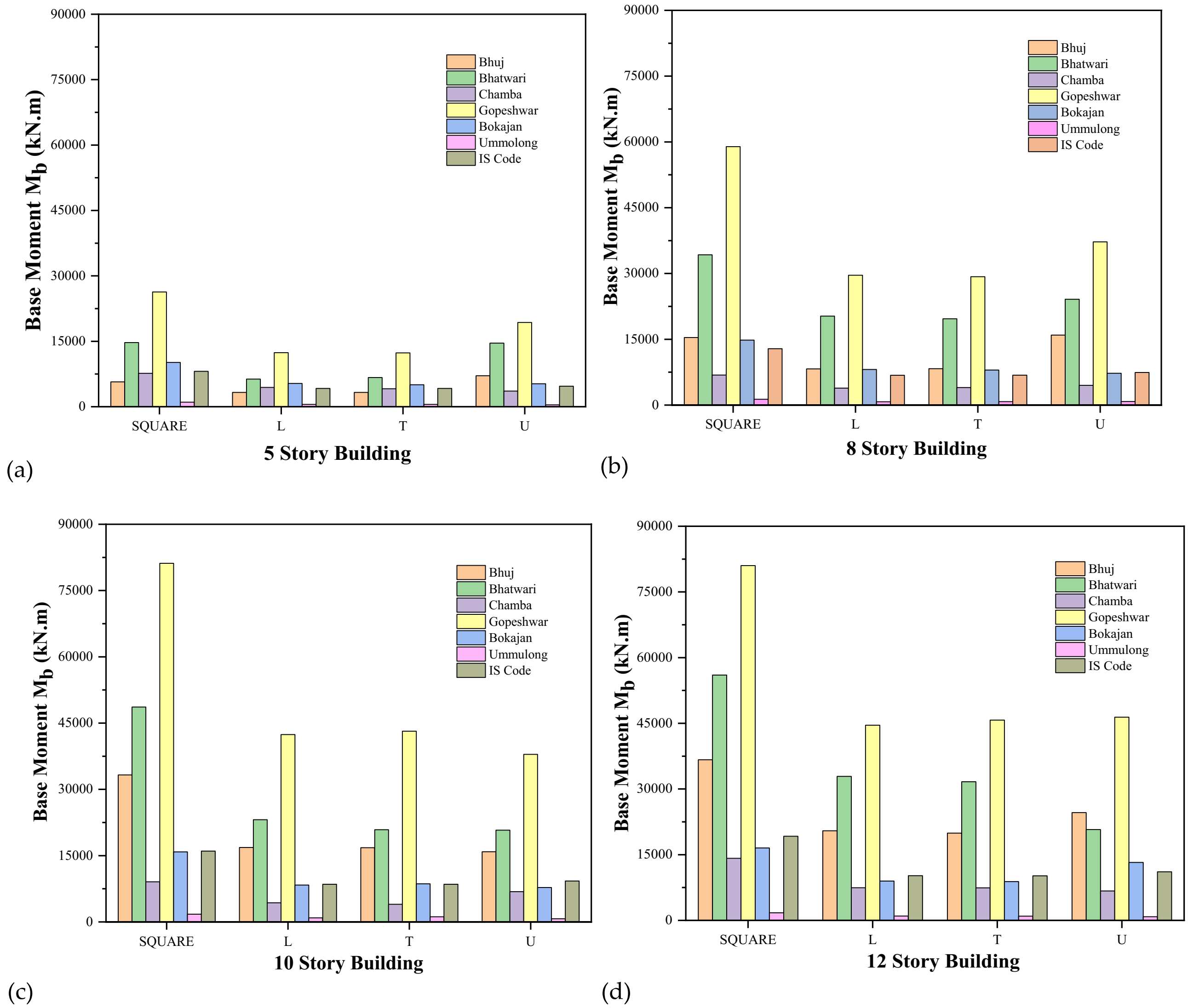

Fig. 9 Base moments for ground accelerations in y direction

6.4 Base moment

Base moment of each mode is obtained by multiplying the corresponding base shear with its center of gravity distance from the structure base. The variation of base moment of all models is almost very similar to that of base shear as these two are linearly proportional. Base moment of almost all the buildings due to Gopeshwar ground motion attains highest value among all the considered ground accelerations. IS 1893:2016 and Ummulong give least value. The 10-story square-shaped rectangular building subjected to Gopeshwar ground motion attains highest value of base moment and is equal to 81165.200 kN.m. Almost same value of base moment, i.e., 81005.653 kN.m, was attained in the same shaped building of 12-story subjected to same ground acceleration. The variations of base moments for ground accelerations in the y direction are presented in Fig. 9.

6.5 Base torsion

Earthquake induces torsion in building due to the eccentricity of masses and stiffness, in addition to the unsymmetrical plan. Accidental torsion is typically used to describe the torsional motion of buildings with ostensibly symmetrical plans, such as the square building. A small portion of the structure's overall seismic forces are produced by this motion.

Table 5 Calculation of seismic response quantities for various 5-story buildings

Mode No.	Base shear (kN)				Base moment (kN.m)				Torsion (kN.m)			
	Type of building				Type of building				Type of building			
	Square	L	T	U	Square	L	T	U	Square	L	T	U
1	487.982	200.569	286.888	596.776	5708.780	2284.546	3267.827	7074.005	–	305.617	275.663	1706.580
2	57.298	204.365	26.231	42.274	– 250.539	2327.798	298.441	500.176	–	00.000	366.396	677.250
3	12.962	31.776	30.667	42.634	43.190	361.649	106.828	127.725	–	424.096	30.690	104.739
4	30.736	21.426	20.548	40.994	– 12.855	74.591	60.902	70.701	–	36.324	26.022	107.707
5	00.709	21.836	70.933	12.669	30.038	76.074	27.888	45.300	–	00.000	50.808	24.283
6	–	30.068	00.771	10.719	–	90.122	20.684	60.160	–	28.422	60.773	22.261
7	–	50.543	20.982	40.960	–	19.462	90.013	15.846	–	60.242	10.900	70.270
8	–	50.641	00.877	10.797	–	19.829	50.116	70.257	–	00.000	00.916	20.581
9	–	00.894	00.309	00.685	–	30.150	10.253	20.851	–	70.731	20.594	60.927
10	–	20.087	00.088	00.269	–	60.310	00.612	10.298	–	10.996	00.723	20.015
11	–	20.120	–	–	–	60.407	–	–	–	00.000	-	–
12	–	00.356	–	–	–	10.368	–	–	–	30.020	-	–
13	–	00.617	–	–	–	30.578	–	–	–	00.792	-	–
14	–	00.622	–	–	–	30.643	–	–	–	00.000	-	–
15	–	00.102	–	–	–	00.694	–	–	–	00.873	-	–
CQC	492.319	289.864	289.850	599.969	5711.956	3283.404	3283.283	7092.944	-	524.872	460.366	1842.480

Unintentional torsion provided around 4% of the overall force for the structure and earthquake under consideration, while other buildings' seismic responses have marked bigger contributions. Because (1) the rotational base motion is not defined and (2) it is impractical to identify and analyze the impact of each source of asymmetry in a building with a nominally symmetrical plan, the structural response associated with accidental torsion cannot be calculated in structural design. For this reason, in this research, the square buildings are considered free of torsion, as indicated in Table 5. Figure 10 shows variation of base torsions based on the type of buildings, ground accelerations, and number of stories. Gopeshwar ground acceleration provides highest value of base torsion, comparing all the ground accelerations. Base torsion was calculated according to IS 1893:2016, and Ummulong gives the least value. The 'U'-shaped building having 12 stories subjected to Gopeshwar ground acceleration provides high value of base torsion, and the value is equal to 6971.374 kN.m. The 'T'-shaped building displays less torsion among unsymmetrical buildings. The 5th, 8th, 10th, and 12th stories of the 'U'-shaped buildings subjected to Gopeshwar ground acceleration provide base torsions of 6096.483 kN.m, 7907.421 kN.m, 7700.633 kN.m, and 6971.374 kN.m, respectively. It clearly points out that base torsion increases as the number of stories increases from 5 to 8, while it then decreases from 8 to 12 stories. Therefore, it attains the second maximum torsion value at the 5-story building. It is mainly due to the lower dynamic response in the 10 and 12-story buildings owing to the reduced spectral accelerations corresponding to the natural time periods. The base torsions of the 'T' and 'L'-shaped buildings are 65% to 70% less than that of the U-shaped building. The results obtained from Khanal and Chaulagain [4] state that the torsional irregularity increases as the plan irregularity increases. In the present study, base torsions in the 'U'-shaped building are 70% to 75% greater than those in the 'T' and 'L'-shaped buildings.

6.6 Inter-story drift

The story drifts in any story subjected to a horizontal design force should not exceed 0.004 times the height of the story, as mentioned in IS 1893:2016 (part 1). The permissible drift ratio is 0.004 (100%) and it is clear that from the first floor to the fourth floor, the inter-story drift values are more than 0.004. This demonstrates that it exceeds the permissible limit. As the first floor displays the maximum drift ratio, it has been compared in all the 12-story buildings subjected to Gopeshwar ground acceleration. The inter-story drift ratios in the 'L', 'T', 'U', and square-shaped buildings are 153.62%, 153.77%, 211.52%, and 151.6%, respectively. Figure 11 displays that the irregular building provides 50% to 110% more inter-story drift than the permissible limit mentioned by IS 1893:2016. While comparing the results obtained from Khanal and Chaulagain [4], it is clear that the inter-story drifts in irregular buildings are 30% more than that in the reference model.

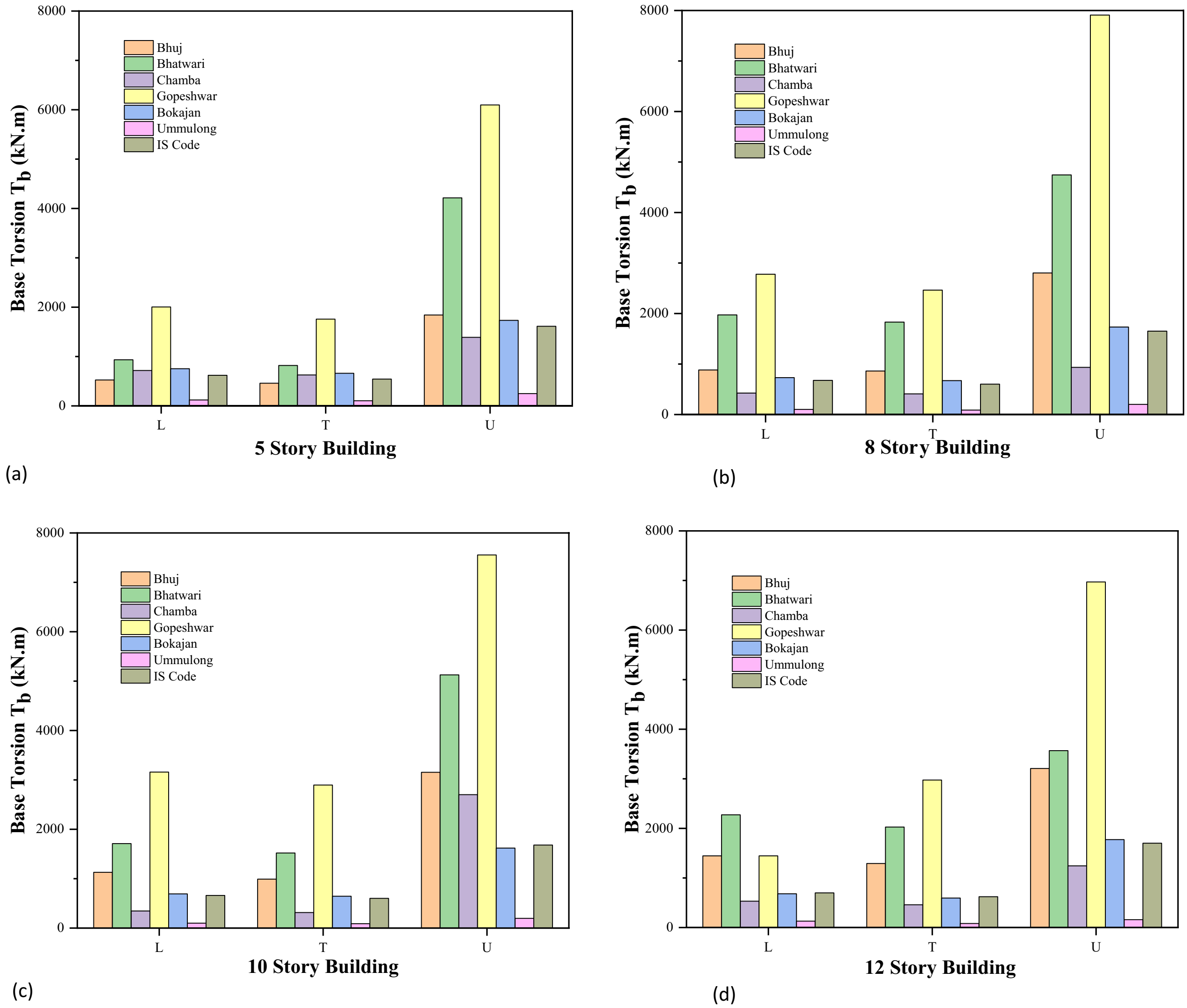

Fig. 10 Base torsions of various unsymmetrical buildings of different stories

6.7 Roof rotation

In all the irregular buildings, the maximum roof rotation is due to Gopeshwar ground acceleration among the considered ground accelerations. In the 5-story building, Bhatwari ground acceleration leads to other ground accelerations, inducing maximum roof rotation in all the irregular buildings. While considering Gopeshwar ground acceleration in the 12-story buildings, roof rotations for the 'L', 'T', and 'U'-shaped buildings are 1.322 rad, 1.470 rad, and 1.871 rad, respectively. Since the square-shaped building is symmetrical about both the x and y axes, it will not induce any rotation. Different ground accelerations, mainly Gopeshwar, Bhuj, along with Bhatwari, induce maximum roof rotations in the 5, 8, 10 and 12-story buildings. It is owing to the high randomly distributed spectral acceleration against the natural time period for different ground accelerations.

While comparing roof rotations among all the 5, 8, 10, and 12-story buildings, the 'U'-shaped building provides 30% to 70% maximum rotation than the 'L' and 'T'-shaped buildings, and the 'L'-shaped building has the least roof rotation. Comparing the results obtained from Khanal and Chaulagain, [4], it is revealed that roof rotation in irregular buildings increases 12% more than the reference models. In this study, roof rotations in the 'U'-shaped building are 30% to 70% greater than those in the 'L' and 'T'-shaped buildings, as depicted in Fig. 12.

Fig. 11 Inter-story drifts of unsymmetrical multi-story buildings of different stories

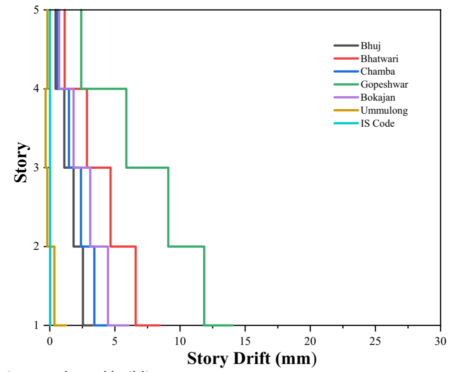

Square-shaped building

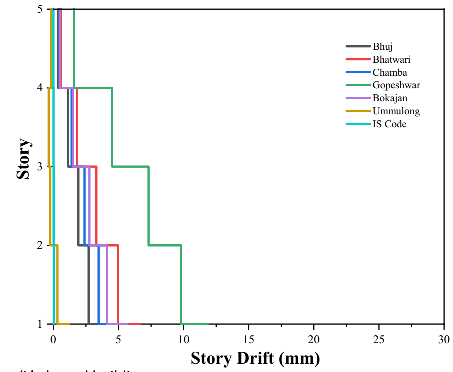

'L'-shaped building

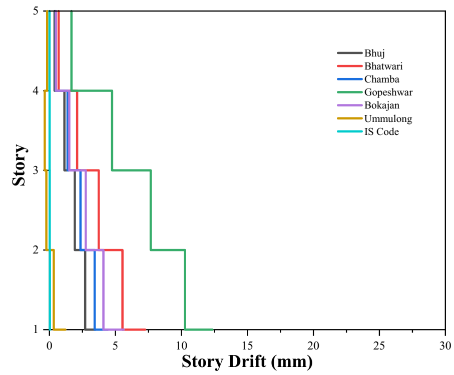

'T'-shaped building

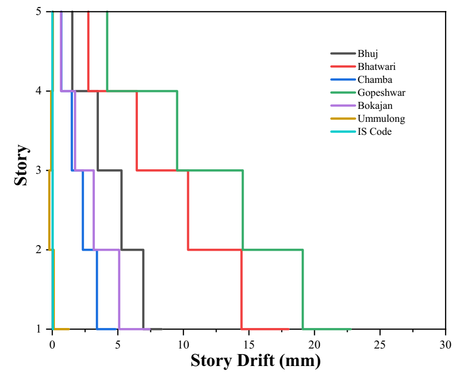

'U'-shaped building

(a) Story drift of 5-story unsymmetrical buildings

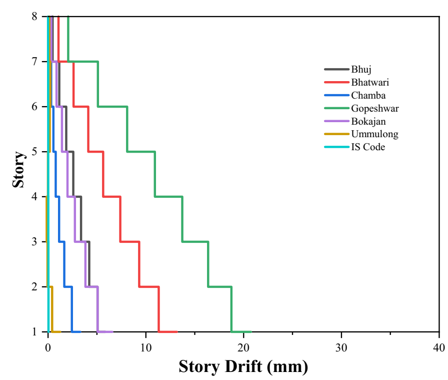

Square-shaped building

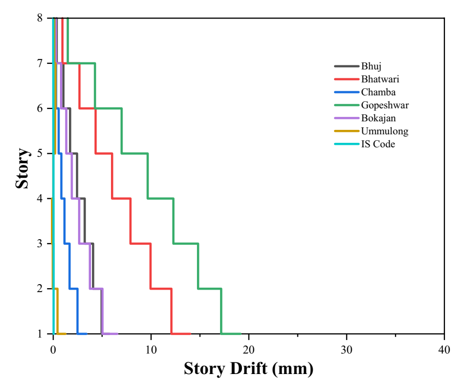

'L'-shaped building

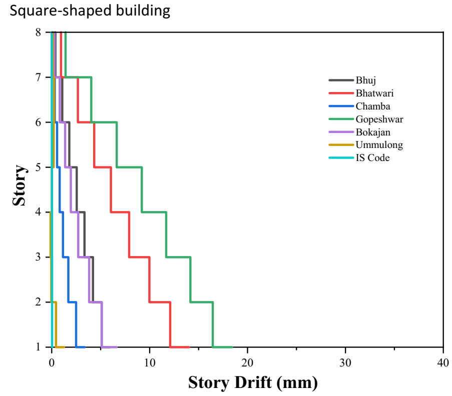

'T'-shaped building

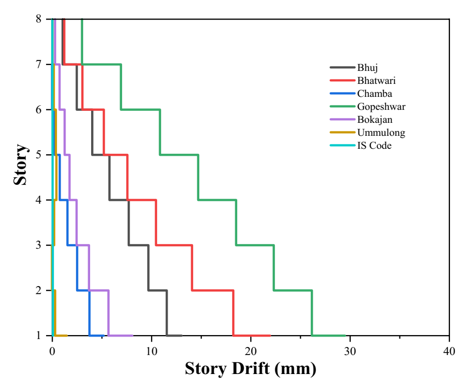

'U'-shaped building

(b) Story drift of 8-story unsymmetrical buildings

Fig. 11 (continued)

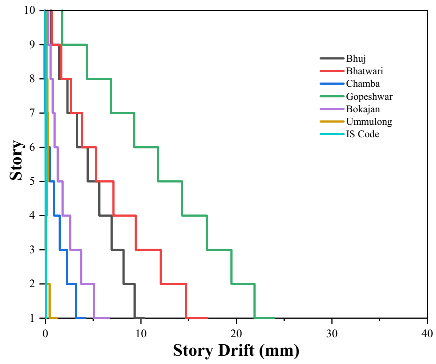

Square-shaped building

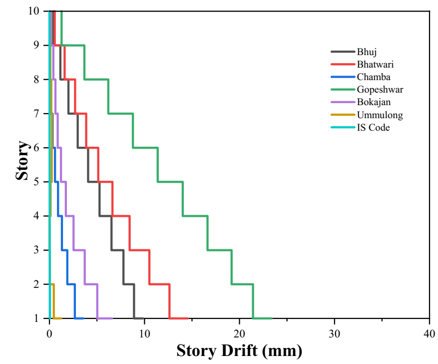

'L'-shaped building

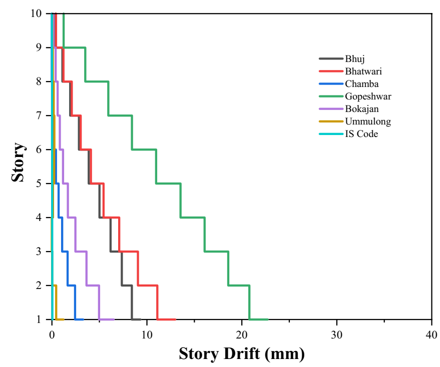

'T'-shaped building

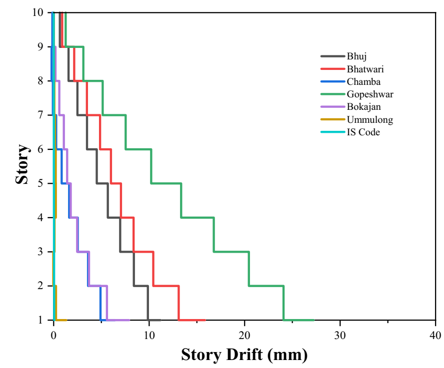

'U'-shaped building

(c) Story drift of 10-story unsymmetrical buildings

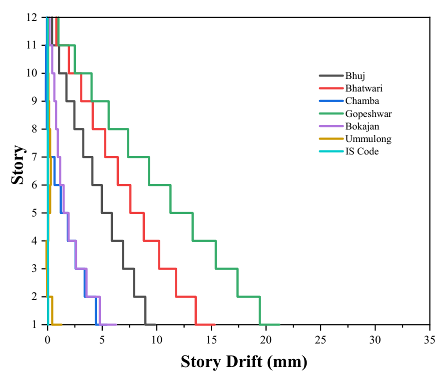

Square-shaped building

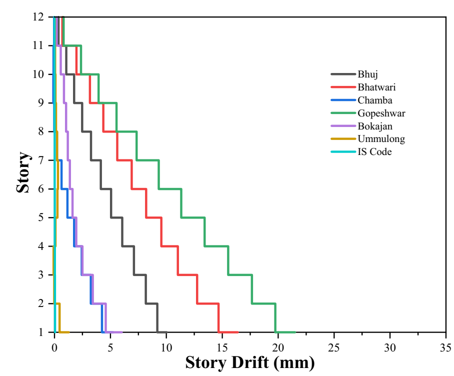

'L'-shaped building

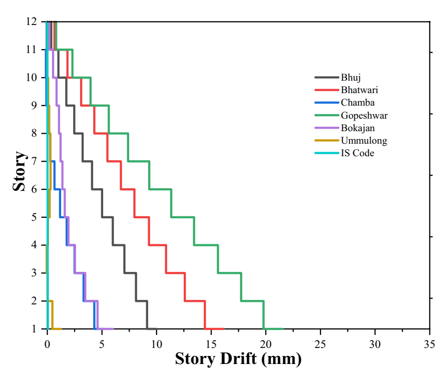

'T'-shaped building

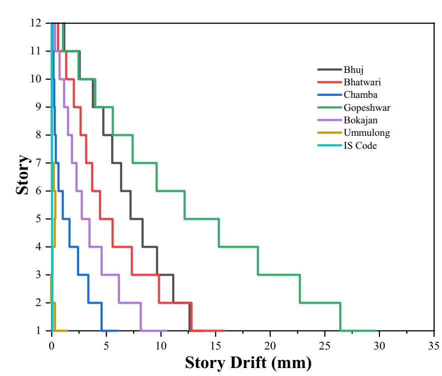

'U'-shaped building

(d) Story drift of 12-story unsymmetrical buildings

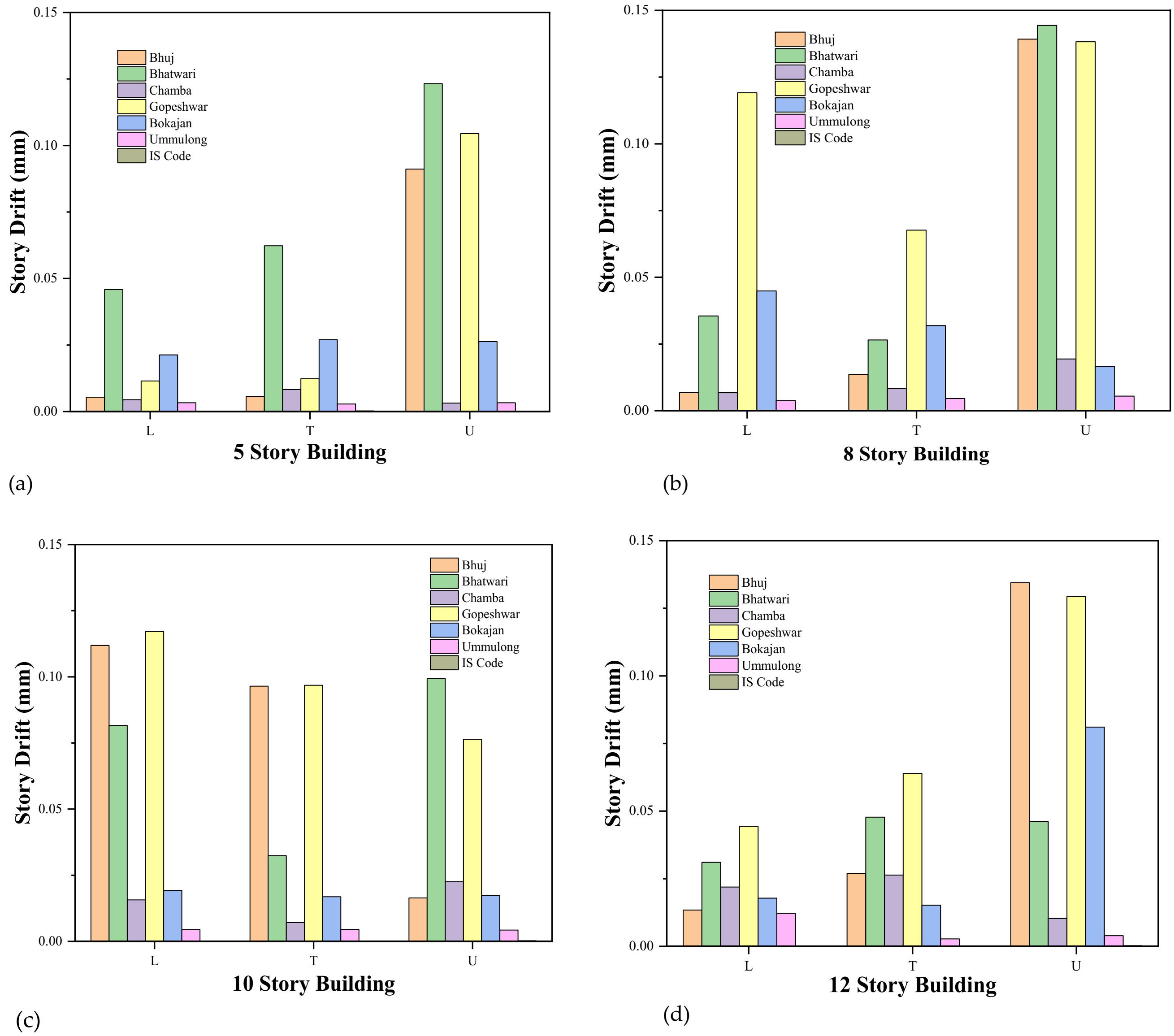

Fig. 12 Story drift in θ direction

6.8 Roof displacement

Roof displacement increases linearly based on the increment of the number of stories of all types of the buildings subjected to all the considered ground accelerations. The 'U'-shaped buildings attain maximum roof displacement among all the buildings. Meanwhile, roof displacements in the 'L' and 'T'-shaped building are lower than those in the reference building; the square-shaped building is taken as the reference building. The maximum roof displacements at the 12-story square, 'L', 'T', and 'U'-shaped buildings due to Gopeshwar ground motion are 134.045 mm, 133.341 mm, 134.089 mm, and 164.801 mm, respectively.

The 'T'-shaped building yielded 13% less roof displacement than the square buildings. Thus, the 'T'-shaped buildings lie within safer side when compared to other buildings. Meanwhile, the 'U'-shaped building displays 50% to 100% more roof displacement than the square-shaped building, hence, it is vulnerable to all other buildings. Comparing the results obtained from Khanal and Chaulagain, [4], it is found that roof displacements in irregular buildings are 20% more than that in the reference model. In this study, roof displacement in the 'U'-shaped building is 50% to 100% greater than the square-shaped buildings, as shown in Fig. 13 for different ground motions.

6.9 Performance level

ATC40 [44] guideline was studied before conducting the pushover analysis on the selected multi-story buildings using ETABS software. The pushover analysis results have been checked to ensure that the nonlinearity is accurately captured. It is possible that the current results appear lightly beyond elastic due to conservative modeling assumptions or an underestimation of plastic hinge properties. In addition, fixation of target displacement as 0.8% of total height of the building, i.e., pushover analysis was not extended until the collapse of the building. But performance points were achieved for all types of the buildings except the 'L'-shaped 5-story and 'U'-shaped 12-story buildings. All the buildings crossed the elastic status. The attainment of the performance point for the 'U'-shaped 10-story building from ETABS software is depicted in Fig. 14.

The location of hinges in various stages can be obtained from pushover curve. The range AB is elastic range, B to IO is the range of IO, IO to LS is the range of LS, and LS to CP is the range of CP mentioned by ATC 40. If all the hinges are within the CP limit, then the structure is said to be safe. However, depending upon the importance of structure, the hinges after the IO range may also need to be retrofitted. Here, when comparing the performance point of all buildings, the 'U'-shaped buildings perform to the maximum shear force. Ruggieri and Uva [40] highlighted the significant impact that the choice of control node can have on the pushover analysis results. The conventional choice is to place the control node at the center of mass of the last story, but this can lead to non-conservative results, particularly for buildings with in-plan irregularities.

On comparing the performance level, base shears in the 10-story buildings such as the square, 'L', 'T' and 'U'-shaped buildings are 100%, 47.21%, 47%, and 65.38%, respectively, i.e., base shear of the square-shaped building is taken as 100 % after assuming it as the reference one. The above discussion indicated that the 'U'-shaped building has 20% to 25% more performance than the 'L' and 'T'-shaped buildings. The performance of symmetrical building is better than unsymmetrical building. The 'L'-shaped building with 5 stories and 'U'-shaped building with 12 stories do not reach their performance points. While comparing the results of Palagala and Singhal [3] with the current study, the performance of infilled reinforced concrete frame increases the seismic performance level than bare-framed buildings. Dalal and Dalal [6] suggested that PBPD-IO does not achieve its performance level whereas in this study the 'L'-5 and 'U'-12-story buildings do not achieve their performance levels. Dalal and Dalal [6] reported that the FBD frame is found to be vulnerable to damage whereas in this study, the 'L'-shaped buildings are highly vulnerable. Hareen and Mohan [7] discussed that while considering the 'L', 'T' and 'U'-shaped buildings, performance points are obtained at peak ground accelerations of 0.16 g, 0.24 g, and 0.36 g, respectively. In this study, for the 10-story buildings of the 'L', 'T' and 'U'-shaped plans, the performance points are achieved at peak ground accelerations of 0.585 g, 0.582 g, and 0.572 g, respectively, as listed in Table 6. Figure 15 illustrates the capacity curves for the 5, 8, 10 and 12-story buildings.

Based on the plastic hinge formation status, it is found that the 'L'-8 story, 'T'-8 story, and 'T'-12 story buildings perform well, as their performance lies within LS in the nonlinear static analysis. The nonlinear performance of the buildings is presented in Table 6.

7 Conclusions

This article presented and discussed the seismic performance of different unsymmetrical buildings such as 'L', 'T', and 'U'-shapes along with square-shaped buildings with varying stories, i.e., 5, 8, 10, and 12 stories. Initially, 6 ground accelerations of various earthquakes from zone V and IS 1893:2016 (rocky soil) data were selected to frame an elastic response spectrum utilizing PRISM software. Response spectrum analysis was carried out for all the buildings to calculate base shear, base moment, base torsion, roof displacement, roof rotation, and story drift. Seismic response of all the buildings was investigated. The following conclusions can be made:

- Even though the square-shaped buildings are symmetrical about both axes, their seismic responses such as base shear and base moment, are greater than those of unsymmetrical plan buildings, such as the 'L' and 'T'-shaped buildings, because seismic weights of the square-shaped buildings are approximately twice those of the 'L' and 'T'-shaped buildings. Total story drift response exceeds the allowable limit as per IS 1893:2016 (part 1) for all types of the buildings, and it reaches the maximum value for the 'U'-shaped building. It is around 110% higher for the 'U'-shaped building and 50% for all other buildings. Regarding roof displacement, the 'U'-shaped building of 12

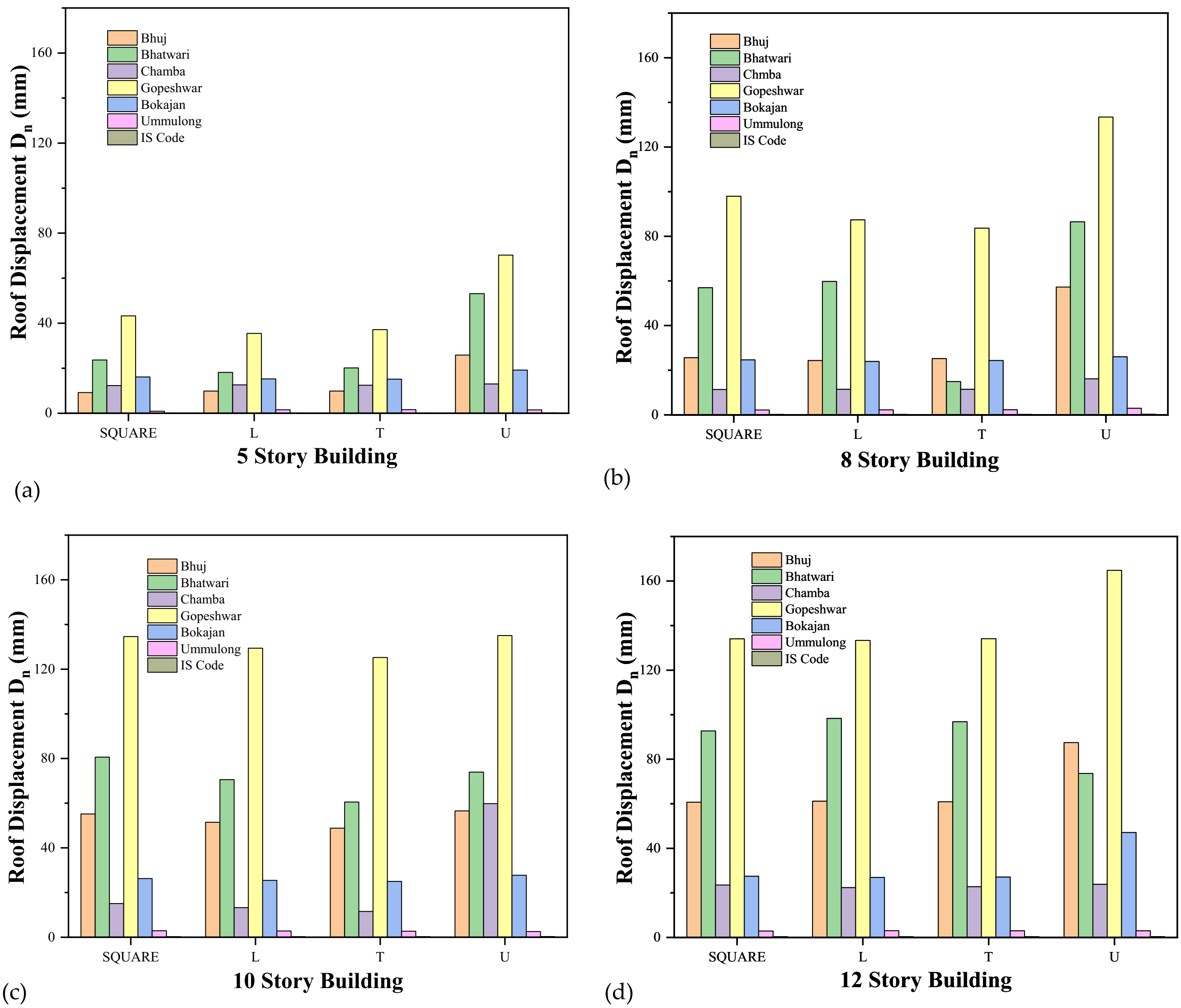

Fig. 13 Roof displacements of various buildings for ground accelerations in y direction

stories attains maximum value of 165 mm. Therefore, concerned with the shape of the irregular buildings, the 'U'-shaped building is more vulnerable than all other irregular buildings.

- The seismic responses given by the x component ground accelerations are less than those by the y component ground accelerations. This is the case for all the buildings, except the square-shaped building which is unsymmetrical about the y axis. On comparing the ground accelerations, Gopeshwar ground acceleration provides maximum seismic responses compared to any other ground accelerations because natural time periods of the first few models of all the buildings are located in the acceleration-sensitive region of this ground acceleration.
- It is known from the nonlinear static analysis that all the 12-story buildings achieve the hinge status of greater than CP, and this hinge state occurs in maximum number of the 'U' and 'L'-shaped buildings, followed by the 'T'-shaped building. It delineates that the 'U'-shaped building is highly susceptible to earthquakes.
- Even though the static response of the 12-story square-shaped building is maximum, its dynamic response, i.e., spectral acceleration, of the first two modes is considerably less when compared to that of a 10-story building. As a result of high randomly distributed spectra acceleration, the increased static response is balanced by the reduced dynamic response. Therefore, base shears as well as base moments of some buildings of 12-story, mainly the square-shaped building, are less than those of the same buildings of 10-story.

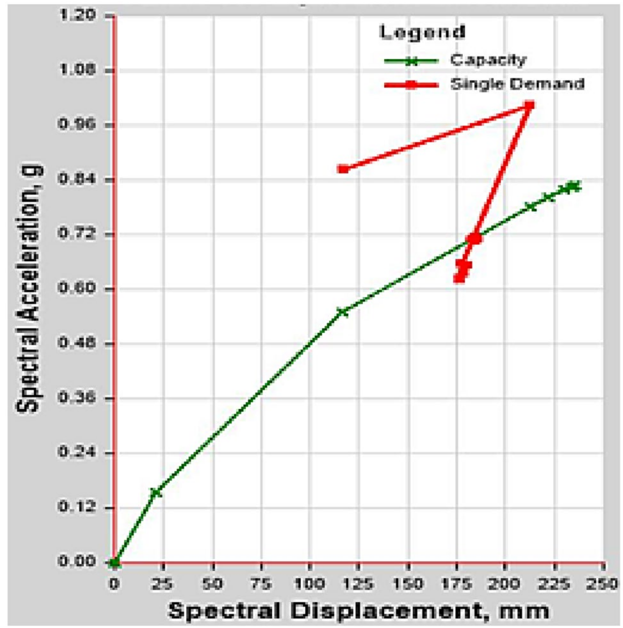

Fig. 14 Performance point for 'U'-shaped 10-story building

Table 6 Performance points and hinge status

Plan-story	Performance point				Hinge status	
	Base shear (kN)	Displacement (mm)	S_a (g)	S_d (mm)		
L-5	–	–	–	–	–	–
L-8	16,115.0712	217.646	0.723663	180.87	B to < = C	IO to < = LS
L-10	16,296.5994	281.13	0.585456	234.672	B to < = C	> CP
L-12	16,003.5672	-334.891	0.480293	279.427	B to < = C	> CP
S-5	30,722.1231	-121.526	1.057843	98.532	B to < = C	> CP
S-8	33,075.3666	-222.36	0.711615	180.931	B to < = C	LS to < = CP
S-10	34,516.4761	-296.139	0.594237	240.937	B to < = C	LS to < = CP
S-12	34,946.8691	-363.079	0.502187	294.945	B to < = C	> CP
T-5	15,251.442	-121.277	1.104953	98.877	B to < = C	> CP
T-8	16,157.8588	-222.267	0.72408	181.615	B to < = C	IO to < = LS
T-10	16,226.3046	-285.073	0.582238	233.094	B to < = C	> CP
T-12	16,223.7564	-347.92	0.486044	284.247	B to < = C	A to < = IO
U-5	21,760.4786	-126.28	1.103064	**99.902**	B to < = C	> CP
U-8	22,509.9716	-224.265	0.712308	183.653	B to < = C	> CP
U-10	22,569.1287	-285.032	0.572128	235.451	B to < = C	> CP
U-12	–	–	–	–	–	–

- Fundamental natural time periods gradually increase when the number of story increases from 5 to 12 for all the buildings. Fundamental natural time periods of the 12-story 'U'-shaped building is maximum among all the buildings and is equal to 1.233 sec. Therefore, it is concluded that the shape and the number of stories of the buildings influence natural time periods which, in turn, affect their spectral accelerations.
- Base torsions in the 'T' and 'L'-shaped buildings are 65% to 70% less than that in the 'U'-shaped building. Due to the less amount of dynamic response in the 10 and 12-story buildings beacuse of the reduced spectral accelerations corresponding to the natural time periods, base torsions of all the unsymmetrical buildings decrease from 8 to 12 stories.

Fig. 15 Capacity curves for various multi-story buildings

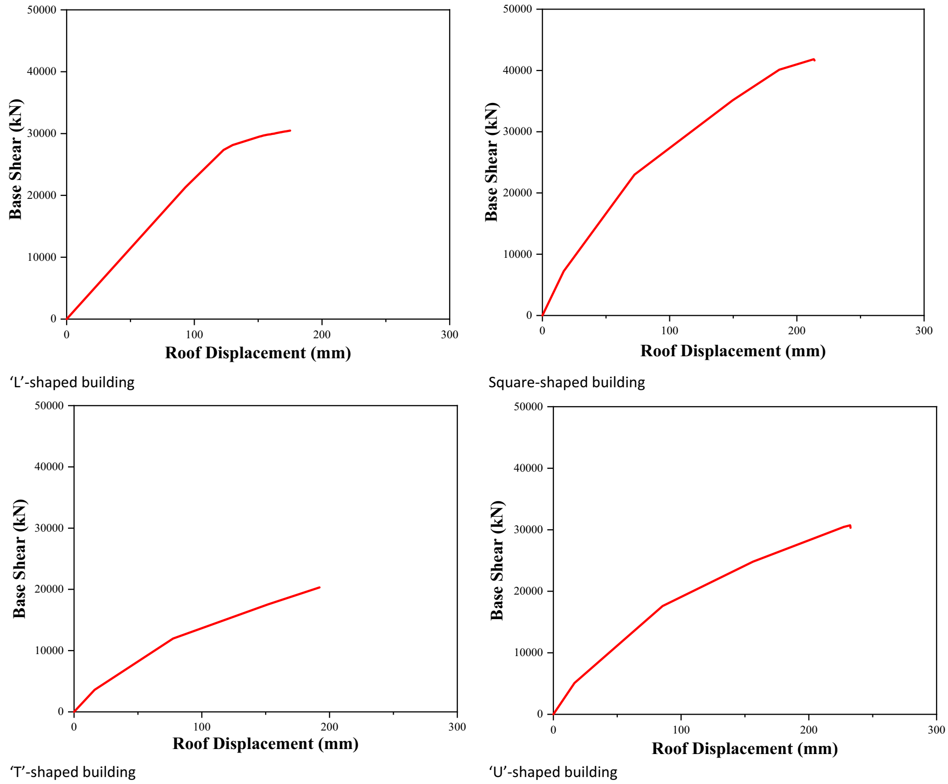

'L'-shaped building

Square-shaped building

'T'-shaped building

'U'-shaped building

(a) Capacity curve for 5-story buildings

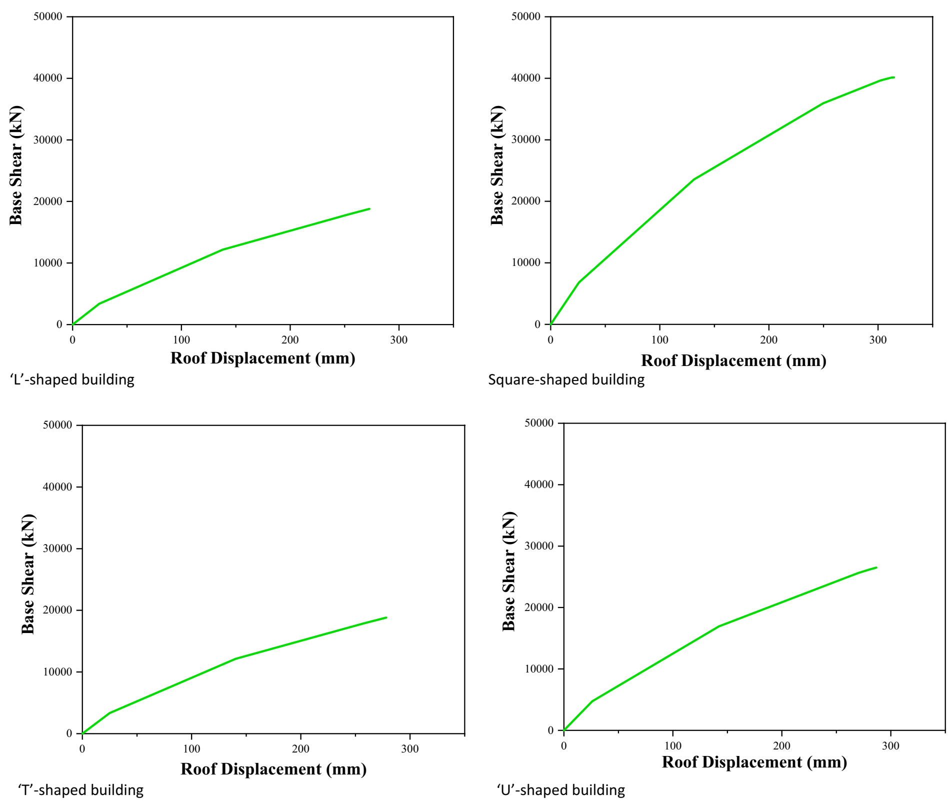

'L'-shaped building

Square-shaped building

'T'-shaped building

'U'-shaped building

(b) Capacity curve for 8-story buildings

Fig. 15 (continued)

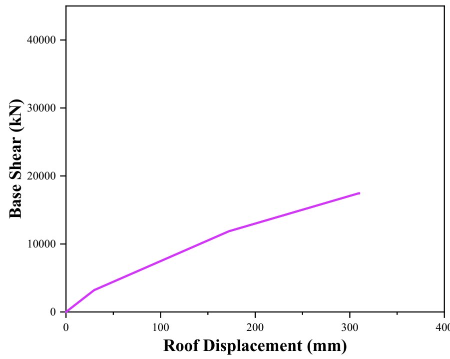

'L'-shaped building

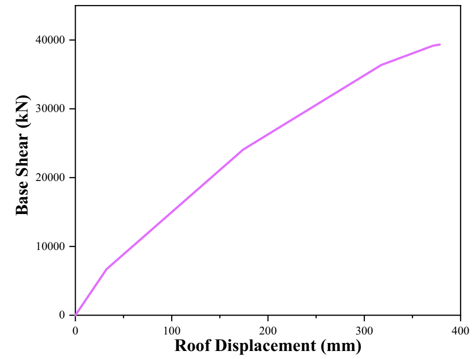

Square-shaped building

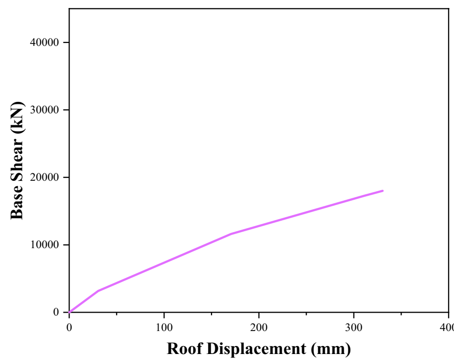

'T'-shaped building

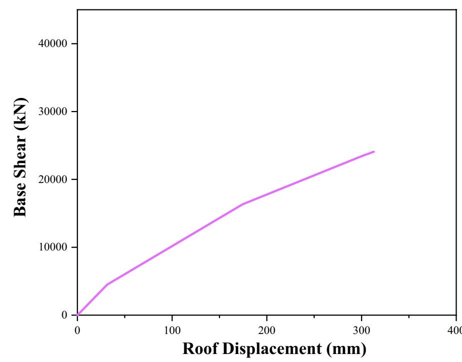

'U'-shaped building

(c) Capacity curve for 10-story buildings

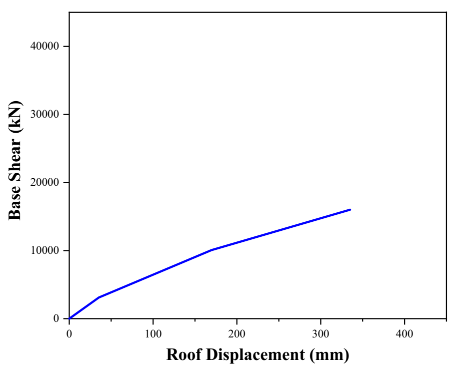

'L'-shaped building

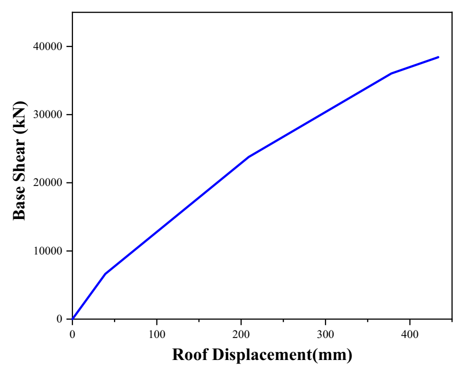

Square-shaped building

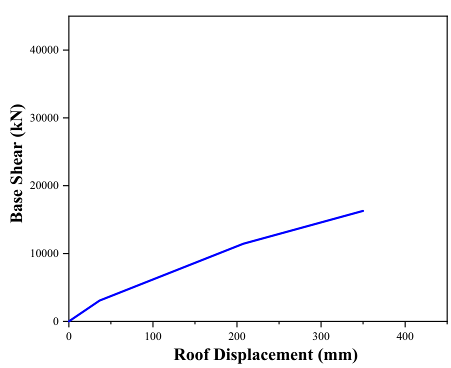

'T'-shaped building

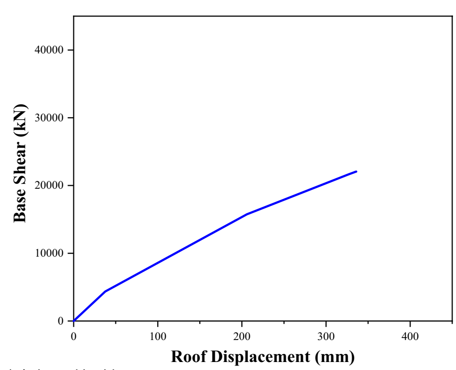

'U'-shaped building

(d) Capacity curve for 12-story buildings

Author contributions Antony Vimal Paul Pandian-Conceptualization, methodology, investigation, software, data curation, validation, formal analysis, visualization, writing—original draft preparation, writing—review and editing. Krishna Prakash Arunachalam-Conceptualization, methodology, investigation, software, data curation, validation, formal analysis, visualization, writing—original draft preparation, writing—review and editing. Alireza Bahrami-Conceptualization, methodology, investigation, software, data curation, validation, formal analysis, visualization, writing—original draft preparation, writing—review and editing. Lenin Miguel Bendezu Romero-Methodology, investigation, software, data curation, validation, formal analysis, writing—original draft preparation, writing—review and editing. Siva Avudaiappan-Conceptualization, investigation, software, data curation, validation, formal analysis, writing—original draft preparation, writing—review and editing. Paul O. Awoyera-Conceptualization, methodology, validation, formal analysis, writing—original draft preparation, writing—review and editing.

Funding Open access funding provided by University of Gävle. No funding was received for conducting this study.

Data availability The authors declare that the data supporting the findings of this study are available within the article.

Code availability Not applicable.

Declarations

Ethics approval and consent to participate Not applicable

Competing interests The authors have no competing interests to declare that are relevant to the content of this article.

References

1. Chopra AK. *Dynamics of Structures, Pearson 5th Edition SI Units Anil K Chopra*; 2012. 53
2. Duggal SK. *Earthquake Resistant Design of Structures*; Oxford University Press, 2007. ISBN 0195688171, 9780195688177, 448 pages.
3. Palagala VY, Singhal V. Structural score to quantify the vulnerability for quick seismic assessment of RC framed buildings in India. Eng Struct. 2021;243:112659. https://doi.org/10.1016/j.engstruct.2021.112659.
4. Khanal B, Chaulagain H. Seismic elastic performance of L-shaped building frames through plan irregularities. Structures. 2020;27:22–36. https://doi.org/10.1016/j.istruc.2020.05.017.
5. Kumar P, Samanta A. Seismic fragility assessment of existing reinforced concrete buildings in Patna India. Structures. 2020;27:54–69. https://doi.org/10.1016/j.istruc.2020.05.036.
6. Dalal SP, Dalal P. Strength, deformation and fragility assessment of reinforced concrete moment resisting frame designed by force based design and the performance based plastic design method for seismic loads. Structures. 2021;29:1154–64. https://doi.org/10.1016/j.istruc.2020.11.029.
7. Hareen CBV, Mohan SC. Evaluation of seismic torsional response of ductile RC buildings with soft first story. Structures. 2021;29:1640–54. https://doi.org/10.1016/j.istruc.2020.12.031.
8. Zameeruddin M, Sangle KK. Performance-based Seismic assessment of reinforced concrete moment resisting frame. J King Saud Univ Eng Sci. 2021;33:153–65. https://doi.org/10.1016/j.jksues.2020.04.005.
9. Sattar S. Evaluating the consistency between prescriptive and performance-based seismic design approaches for reinforced concrete moment frame buildings. Eng Struct. 2018;174:919–31. https://doi.org/10.1016/j.engstruct.2018.07.080.
10. Cardone D, Flora A. Multiple inelastic mechanisms analysis (MIMA): a simplified method for the estimation of the seismic response of RC frame buildings. Eng Struct. 2017;145:368–80. https://doi.org/10.1016/j.engstruct.2017.05.026.
11. Bhasker R, Menon A. Torsional irregularity indices for the seismic demand assessment of RC moment resisting frame buildings. Structures. 2020;26:888–900. https://doi.org/10.1016/j.istruc.2020.05.018.
12. Chandra Dutta S, Halder L, Prasad Sharma R. Seismic vulnerability assessment of low to mid-rise RC buildings addressing prevailing design and construction practices in the Northeastern region of the Indian subcontinent: a case study based approach. Structures. 2021;33:1561–77. https://doi.org/10.1016/j.istruc.2021.05.032.
13. Gautam D, Adhikari R, Rupakhety R. Seismic fragility of structural and non-structural elements of Nepali RC buildings. Eng Struct. 2021;232:111879. https://doi.org/10.1016/j.engstruct.2021.111879.
14. Divyah N, Prakash R, Srividhya S, Avudaiappan S, Guindos P, Carsalade NM, Arunachalam KP, Noroozinejad Farsangi E, Roco-Videla Á. Experimental and numerical investigations of laced built-up lightweight concrete encased columns subjected to cyclic axial load. Buildings. 2023;13:1444.
15. Arunachalam KP, Sukumaran M. Crack failure analysis of scaffolding frame intersection using ADINA. Mater Sci Res India. 2017;14:47–51.

16. Dutta SC, Jangid R, Mandal P, Arora RK. Influence of strength dependent stiffness on seismic design. Eng Struct. 2021;227:111444. https://doi.org/10.1016/j.engstruct.2020.111444.
17. Mostafijur Rahman M, Jadhav SM, Shahrooz BM. Seismic performance of reinforce concrete buildings designed according to codes in Bangladesh India and U.S. Eng Struct. 2018;160:111–20. https://doi.org/10.1016/j.engstruct.2018.01.010.
18. Oggu P, Gopikrishna K. Assessment of three-dimensional RC moment-resisting frames under repeated earthquakes. Structures. 2020;26:6–23. https://doi.org/10.1016/j.istruc.2020.03.039.
19. Bhasker R, Menon A. Characterization of ground motion intensity for the seismic fragility assessment of plan-irregular RC buildings. Structures. 2020;27:1763–76. https://doi.org/10.1016/j.istruc.2020.08.019.
20. Hussain MA, Dutta SC. Inelastic seismic behavior of asymmetric structures under bidirectional ground motion: an effort to incorporate the effect of bidirectional interaction in load resisting elements. Structures. 2020;25:241–55. https://doi.org/10.1016/j.istruc.2020.03.014.
21. Zain M, Usman M, Hassan Farooq S. A framework with reduced computational burden for seismic fragility assessment of reinforced concrete buildings in high-intensity seismic zones. Structures. 2021;33:3055–65. https://doi.org/10.1016/j.istruc.2021.06.050.
22. Surana M, Singh Y, Lang DH. Effect of structural characteristics on damping modification factors for floor response spectra in RC buildings. Eng Struct. 2021;242:112514. https://doi.org/10.1016/j.engstruct.2021.112514.
23. Jalilkhani M, Ghasemi SH, Danesh M. A multi-mode adaptive pushover analysis procedure for estimating the seismic demands of RC moment-resisting frames. Eng Struct. 2020;213:110528. https://doi.org/10.1016/j.engstruct.2020.110528.
24. Belejo A, Bento R. Improved modal pushover analysis in seismic assessment of asymmetric plan buildings under the influence of one and two horizontal components of ground motions. Soil Dyn Earthq Eng. 2016;87:1–15. https://doi.org/10.1016/j.soildyn.2016.04.011.
25. Daei A, Poursha M. On the accuracy of enhanced pushover procedures for seismic performance evaluation of code-conforming RC moment-resisting frame buildings subjected to pulse-like and non-pulse-like excitations. Structures. 2021;32:929–45. https://doi.org/10.1016/j.istruc.2021.03.035.
26. Xu H, Gardoni P. Probabilistic capacity and seismic demand models and fragility estimates for reinforced concrete buildings based on three-dimensional analyses. Eng Struct. 2016;112:200–14. https://doi.org/10.1016/j.engstruct.2016.01.005.
27. Pandian AVP, Arunachalam KP, Avudaiappan S, Jasmin SS, Romero LMB, Awoyera PO. Modification of response reduction factors of overhead water tanks based on ductility factor. Discov Appl Sci. 2024;6:192. https://doi.org/10.1007/s42452-024-05762-z.
28. Kassem MM, Mohamed Nazri F, Noroozinejad Farsangi E. Development of seismic vulnerability index methodology for reinforced concrete buildings based on nonlinear parametric analyses. MethodsX. 2019;6:199–211. https://doi.org/10.1016/j.mex.2019.01.006.
29. Zhang C, Tian Y. Simplified performance-based optimal seismic design of reinforced concrete frame buildings. Eng Struct. 2019;185:15–25. https://doi.org/10.1016/j.engstruct.2019.01.108.
30. Vimal PPA, Regin JJ, Jinu GR, Chettiar CG. Experimental investigation on elevated water tanks with base isolation—response spectrum approach. J Theor Appl Mech. 2020;58:885–99.
31. Vimal PA, Suresh SL, Vinu M. Effects of fundamental natural time periods on the seismic performance of base isolated multistory buildings. Asian J Civ Eng. 2023. https://doi.org/10.1007/s42107-023-00604-6.
32. Li SQ, Chen YS, Liu HB, et al. Empirical seismic vulnerability assessment model of typical urban buildings. Bull Earthquake Eng. 2023;21:2217–57. https://doi.org/10.1007/s10518-022-01585-8.
33. Li SQ, Zhong J. Development of a seismic vulnerability and risk model for typical bridges considering innovative intensity measures. Eng Struct. 2024;302:117431. https://doi.org/10.1016/j.engstruct.2023.117431.
34. Li SQ. A simplified prediction model of structural seismic vulnerability considering a multivariate fuzzy membership algorithm. J Earthq Eng. 2024. https://doi.org/10.1080/13632469.2023.2217945.
35. Li SQ, Li YR, Han JC, Qin PF, Ke D. Seismic hazard models for typical urban masonry structures considering optimized regression algorithms. Bull Earthq Eng. 2024;22:2797–827. https://doi.org/10.1007/s10518-024-01879-z.
36. Li SQ, Du K, Li YR, et al. Seismic vulnerability estimation of RC structures considering empirical and numerical simulation methods. Archiv Civ Mech Eng. 2024;24:68. https://doi.org/10.1007/s43452-024-00874-0.
37. Li SQ. Probabilistic seismic hazard model and vulnerability analysis for typical regional structures. Bull Earthquake Eng. 2024. https://doi.org/10.1007/s10518-024-01938-5.
38. Ruggieri S, Vukobratović V. The influence of torsion on acceleration demands in low-rise RC buildings. Bull Earthquake Eng. 2024;22:2433–68. https://doi.org/10.1007/s10518-024-01873-5.
39. Ruggieri S, Uva G. Extending the concepts of response spectrum analysis to nonlinear static analysis: does it make sense? Innov Infrastruct Solut. 2024;9:235. https://doi.org/10.1007/s41062-024-01561-y.
40. Uva G, Porco F, Fiore A, Ruggieri S. Effects in conventional nonlinear static analysis: evaluation of control node position. Structures. 2018;13:178–92. https://doi.org/10.1016/j.istruc.2017.12.006.
41. Standards, B. (Bureau of I. Criteria for Earthquake Resistant Design of Structure. **2016**, 1–23.
42. IS 875 (part 1) IS 875–1: Code of Practice For Design Loads (Other Than Earthquake)For Buildings And Structures, Part 1: Dead Loads. *Bur. Indian Stand. New Delhi* 1987, *875*, 1–37.
43. IS 875 (part 2)-1987 standard, B. (Bureau of I. Code of Practice for Design Loads (Other than Earthquake) for Buildings and Structures: Imposed Loads. 1987, 18.
44. Applied Technology Council (ATC40)- 1996. Seismic Evaluation and Retrofit of Concrete Buildings Vol.1. California Seismic Safety Commission. 1996, 69.